

Identification of twenty-three accreting binaries in the Galactic Bulge Survey

M.A.P. Torres^{1*}, P.G. Jonker^{1,2,3}, C.T. Britt^{4,5}, C. B. Johnson⁴, R.I. Hynes⁴, S. Greiss⁶,
D. Steeghs⁶, T. J. Maccarone⁵, F. Özel⁷, C. Bassa⁸, G. Nelemans^{3,9}

¹*SRON, Netherlands Institute for Space Research, Sorbonnelaan 2, 3584 CA, Utrecht, The Netherlands*

²*Harvard-Smithsonian Center for Astrophysics, 60 Garden Street, Cambridge, MA 02138, U.S.A.*

³*Department of Astrophysics/ IMAPP, Radboud University Nijmegen, Heyendaalseweg 135, 6525 AJ, Nijmegen, The Netherlands*

⁴*Department of Physics and Astronomy, Louisiana State University, Baton Rouge, LA, 70803-4001, USA*

⁵*Department of Physics, Texas Tech University, Box 41051, Lubbock, TX 79409-1051, USA*

⁶*Department of Physics, University of Warwick, Coventry CV4 7AL, UK*

⁷*University of Arizona, Department of Astronomy, 933 N. Cherry Ave., Tucson, AZ 85721, U.S.A*

⁸*Jodrell Bank Centre for Astrophysics, The University of Manchester, Manchester M13 9PL*

⁹*Institute for Astronomy, KU Leuven, Celestijnenlaan 200D, B-3001 Leuven, Belgium*

29 October 2018

ABSTRACT

We are undertaking a survey to characterize the X-ray sources found with the *Chandra* X-ray observatory in a strip of fields at $-3^\circ < l < 3^\circ$, $b = +1.5^\circ$ and $-3^\circ < l < 3^\circ$, $b = -1.5^\circ$. This so-called Galactic Bulge Survey (GBS) targets X-ray emitting binaries in the bulge with the primary purpose of finding quiescent X-ray binaries. The aims of this survey are to quantify dynamically the mass of compact objects in these X-ray binaries in order to constrain the neutron star equation of state and to test black hole formation models. In addition, using the survey number counts of various sources we aim to test models for binary formation and evolution. Here, we present the identification of optical counterparts to twenty-three GBS X-ray sources. We report their accurate coordinates and medium resolution optical spectra acquired at the Very Large Telescope and Magellan. All sources are classified as accreting binaries according to their emission line characteristics. To distinguish accreting binaries from chromospherically active objects we develop and explain criteria based on H α and He I $\lambda\lambda 5786, 6678$ emission line properties available in the literature. The spectroscopic properties and photometric variability of all the objects are discussed and a classification of the source is given where possible. Among the twenty-three systems, at least nine of them show an accretion-dominated optical spectrum (CX28, CX63, CX70, CX128, CX142, CX207, CX522, CX794 CX1011) and another six show photospheric lines from a late-type donor star in addition to accretion disc emission (CX44, CX93, CX137, CX154, CX377 and CX1004) indicating that they are probably accreting binaries in quiescence or in a low accretion rate state. Two sources are confirmed to be eclipsing: CX207 and CX794. CX207 shows a broad asymmetric H α profile blue-shifted by $> 300 \text{ km s}^{-1}$. Such line profile characteristics are consistent with a magnetic (Polar) cataclysmic variable. CX794 is an eclipsing nova-like cataclysmic variable in the period gap. Time-resolved photometry and the large broadening of the H α emission lines in CX446 (2100 km s^{-1} Full-Width at Half Maximum; FWHM) suggest that this is also an eclipsing or high-inclination accreting binary. Finally, the low-accretion rate source CX1004 shows a double-peaked H α profile with a FWHM of 2100 km s^{-1} . This supports a high inclination or even eclipsing system. Whether the compact object is a white dwarf in an eclipsing cataclysmic variable or a black hole primary in a high-inclination low-mass X-ray binary remains to be established.

Key words: techniques: spectroscopic, photometric, radial velocities; binaries: close; accretion, accretion discs; black hole physics; stars: neutron; X-rays: binaries

1 INTRODUCTION

The Galactic Bulge Survey (GBS) is a multi-wavelength survey designed to search for both X-ray sources and their optical counterparts in the direction towards and in the Milky Way bulge. The GBS covers a pair of $6^\circ \times 1^\circ$ areas centered 1.5° above and below the Galactic Plane. These regions are chosen to avoid the high optical extinction and crowding found in the mid-plane. The full survey area has been observed in X-rays with the *Chandra* X-ray observatory to a 0.5 - 10 keV flux upper limit of $(1 - 3) \times 10^{-14}$ erg cm $^{-2}$ s $^{-1}$. The GBS area has been also imaged in optical bands with the CTIO 4-m Blanco telescope to typical upper limits of r' , $i' \lesssim 23$.

A total of 1640 unique X-ray sources have been found (Jonker et al. 2011; Jonker et al. in prep.), providing a large sample to fulfill the two main goals of this project. In what follows we briefly describe these goals, while the specific details concerning the GBS can be found in Jonker et al. (2011). The first GBS goal involves measuring masses of neutron stars and black holes in eclipsing X-ray binaries in order to constrain the neutron star equation of state and black hole formation models. This requires us to identify new X-ray binaries with optical counterparts suitable for dynamical studies. These studies will allow one to measure the masses of compact objects, with unprecedented accuracy in the case of eclipsing systems. To facilitate achieving this objective, the limiting sensitivity for the X-ray imaging was selected to maximize the number of detected quiescent low-mass X-ray binaries (qLMXBs) with respect to new Cataclysmic Variables (CVs). The expectation is to detect in X-rays more than 200 qLMXBs with 120 of them having detectable counterparts in the GBS optical images. In comparison, the current number of known LMXBs in the Galaxy exceeds 170 (see e.g. Özel et al. 2010). More than half of them are persistently X-ray bright, making them usually unsuitable for dynamical studies due to the lack of spectral features from the donor star in their optical spectra. In contrast, the photosphere from the donor star is expected to contribute significantly to the optical spectra of qLMXBs. Nowadays the census of LMXBs grows each year by a few with the discovery of transient LMXBs during unpredictable X-ray outbursts. Once in quiescence, optical counterparts are detected for sources not affected by severe reddening and/or crowding issues. The GBS instead represents a systematic effort to identify a large sample of new qLMXBs with optical counterparts suitable for further follow-up. A sample consisting of systems that have not undergone a recent outburst will allow us to establish if there exist selection effects that arise from the current sample of persistent objects and transients that have suffered outbursts in the past few decades.

The second GBS objective is to investigate binary formation and evolution scenarios, including the study of kicks during the supernova event that produces the compact primary in an LMXB. The method employed to achieve this goal involves comparing the observed number of sources per source class with the number of sources predicted by binary population synthesis calculations. The calculations presented in Jonker et al. (2011) predicted a total of 1648 X-ray sources in the GBS area. This is in very good agreement with the 1640 sources detected in X-rays. To allow de-

tailed comparisons, multiwavelength and variability studies are in progress to identify and characterize counterparts to the GBS sources. See e.g. Udalski et al. (2012) and Hynes et al. (2012a) for a photometric search and study of GBS sources with bright or moderately bright optical counterparts, Greiss et al. (2013) for the identification of counterparts at infrared bands, Britt et al. (2013) for the optical spectroscopic identification of five accreting binaries, Maccarone et al. (2012b) for the characterization of GBS sources with bright radio counterparts, Ratti et al. (2013a) for the first dynamical study of a GBS source and Hynes et al. (2013) for the identification of a symbiotic X-ray binary. The GBS and related data are also being used to study recently discovered X-ray transients or previously known (but poorly studied) sources showing renewed activity (e.g. Greiss et al. 2011a,b; Hynes et al. 2012a, Maccarone et al. 2012a, Rojas et al. 2012)

In order to identify the optical counterparts we are acquiring spectra for the candidate counterparts found within the error circle for the precise *Chandra* X-ray position. Large aperture telescopes are being used to target qLMXBs which are expected to be faint as they suffer from reddening and are located at kiloparsec distances. For instance the unreddened apparent magnitude and colours of a (donor) star at a distance of 8 kpc are $(r', r' - i', r' - K)_0 = (17.4, 0.1, 0.9)_0$ for F0 dwarfs and $(23.6, 1.3, 3.4)_0$ for M2 dwarfs. Taking into account reddening the predicted apparent magnitudes for active LMXBs in the GBS area is $18 < i' < 21$, while qLMXBs are expected to have $i' > 20$ (Jonker et al. 2011).

In this paper we focus on twenty-three GBS objects that we have selected as new accreting binaries on the basis of our results obtained from spectroscopy with the VLT and Magellan telescopes. We begin by describing in Section 2 the spectroscopic and photometric observations. In Section 3 we explain how the data were processed. In Section 4 we present and discuss the results for the twenty-three sources. Accurate coordinates, finding charts, optical light curves from the Blanco 4m telescope and spectra of medium resolution ($\sim 5, 10 \text{ \AA}$) and relatively large wavelength coverage are provided for each object. Finally, in Section 5 we consider how to overcome the selection bias toward emission line objects that single epoch spectroscopic surveys will suffer from. In this paper we will follow the designation to the sources introduced in Jonker et al. (2001): CX N where N is the source number in the count rate sorted GBS catalogue.

2 OBSERVATIONS AND DATA REDUCTION

2.1 VIMOS (*Visible Multi-Object Spectrograph*)

VIMOS (Le Fèvre et al., 2003) is a 4-channel imager and multi-object spectrograph mounted on the Nasmyth focus of the 8.2-m ESO Unit 3 Very Large Telescope at Paranal, Chile. Each channel (a.k.a. quadrant) covers a field of view of about 7×8 arcmin 2 . The four quadrants are separated by approximately 2 arcmin wide gaps. The current VIMOS detectors are 2048×4096 pixels EEV CCDs that provide a 0.205 arcsec/pixel scale. Prior to August 2011 VIMOS was equipped with EEV CCDs of same format as the new detector, but with both lower sensitivity and strong fringing in the red. The GBS sources CX73 and CX772 were observed using the old CCDs.

During the observations VIMOS was operated in multi-object spectroscopy (MOS) mode. In this mode laser-cut slit masks are inserted at the entrance focal plane permitting spectroscopy of optical counterpart candidates to several GBS sources in a single exposure. The slit masks are prepared using the VIMOS Mask Preparation Software (VMMP) tool (see Bottini et al. 2005). VMMP uses pre-images of the fields as reference frames to define the slit and secure objects well-centered at the slit positions after telescope acquisition of the field. All slits were designed with a 1.0 arcsec width. Their length and location were determined per GBS source to include more than one optical counterpart candidates if possible, to secure areas for sky subtraction during the data reduction and/or to avoid strong saturation of bright sources. Thus the identified counterparts were not necessarily centered on their slits.

We selected the medium resolution (MR) grism that yields a $2.5 \text{ \AA}/\text{pixel}$ dispersion and a wavelength coverage of $\sim 4800 - 10000 \text{ \AA}$. The exact coverage depends on the location of the small slit with respect to the CCD boundaries as some part of the dispersed spectrum may fall off the chip. The GG475 order-sorting filter was used to avoid overlap between the first and second grating orders when observing bright sources. The use of 1.0 arcsec width slits provided a spectral resolution of about 10 \AA FWHM corresponding to 460 km s^{-1} at $\text{H}\alpha$ and 350 km s^{-1} at 8600 \AA .

The spectroscopic observations were obtained in service mode under programs 085.D-0441(A) and 087.D-0596(A). One hour observing blocks (OBs) were executed per pointing, consisting of acquisition imaging, two spectroscopic integrations of 875 s, three flat-field exposures and a helium-argon lamp exposure for wavelength calibration. The standard data reduction steps were performed with the ESO-VIMOS pipeline (Izzo et al. 2004). These include bias subtraction, bad-pixel correction, wavelength calibration and removal of the instrumental response. The typical root mean square (RMS) for the wavelength calibration fit was < 0.1 pixels. The pipeline averages the two spectra and extracts automatically the objects found in each slit.

The pipeline data products were examined to identify any problems with the extraction of the spectra. This examination showed that the output spectra for isolated objects were satisfactory in terms of extraction quality. This was not the case for partially resolved sources where the choice of the aperture size for the object, sky subtraction regions and tracing become critical steps during the extraction process. Thus we extracted interactively with the IRAF KPNOSLIT package all reduced 2-D frames that contain both stellar and sky spectra (pipeline files with product code SSEM). For partially resolved sources in crowded fields, the object and sky apertures were sized to maximize the number of pixels contributing to the object and sky, respectively, and to minimize the contribution from any field star/s. Checks for the stability of the wavelength calibration were made for each object looking at the strongest atmospheric emission lines present in the spectra. We made use of the $[\text{O}\text{I}] \lambda 6300.3$ line and/or the OH emission at $\lambda\lambda 6863.96, 9872.14 \text{ \AA}$ (Osterbrock et al. 1996, 1997). In this way we estimate that the median amplitude of the radial velocity error is $\lesssim 20 \text{ km s}^{-1}$. Zero point corrections were applied only to the spectra of the sources CX70 and CX377 which showed radial veloc-

ity offsets in the $[\text{O}\text{I}]$ and OH emission lines wavelengths well above the distribution of the internal radial velocity error.

In a few cases the observing conditions were not good during the OB execution and the OB was repeated later under the weather conditions requested for the program. Spectra of an optical counterpart extracted from different OBs were combined if they were acquired close in time and if there were no significant changes in the spectra between observations. A log of the VIMOS observations is presented in Table 1 in which identification numbers for the GBS sources, pre-imaging OBs and spectroscopic OBs are given. The observing date and the quadrant where the object was detected are also provided.

2.2 IMACS (Inamori-Magellan Areal Camera and Spectrograph)

The GBS sources CX44 and CX1011 were observed with IMACS (Bigelow & Dressler 2003) which is mounted on the 6.5-m Baade-Magellan telescope at Las Campanas Observatory. Both objects were observed on the night of 15 May 2011 UT with IMACS operated in short-camera mode. In this mode the spectra are dispersed along the long axis of two of the eight 2112×4160 pixels E2V CCDs with $0.20 \text{ arcsec/pixel}$ scale. We used a 300 line mm^{-1} grism centered at 6700 \AA yielding a dispersion of $1.15 \text{ \AA pixel}^{-1}$ (CCD No. 3) and $1.31 \text{ \AA pixel}^{-1}$ (CCD No. 8) in the spectral intervals $3450 - 6660$ and $6750 - 10410 \text{ \AA}$, respectively. Together with a 1.0 arcsec wide slit, the instrumental setup achieved a spectral resolution of $\sim 5 \text{ \AA}$ FWHM corresponding to 230 km s^{-1} at $\text{H}\alpha$ and 175 km s^{-1} at 8600 \AA . A single spectrum was acquired per source with an integration time of 1200 and 900 s for CX44 and CX1011, respectively. The flux standards Feige 56, Feige 57 and LTT 3864 were also observed in order to correct for the instrumental response.

The IMACS frames were bias and flat-field corrected with standard IRAF routines. The spectra were extracted from each CCD frame with the IRAF KPNOSLIT package. The pixel-to-wavelength calibration was derived from cubic spline fits to HeNeAr arc lines. The RMS deviation of the fit was $\lesssim 0.06 \text{ \AA}$. The sky $[\text{O}\text{I}] \lambda 6300.3$ line and the OH emission blend at 7316.3 \AA show that the accuracy of the wavelength calibration of the spectra from both CCDs is $\lesssim 0.08 \text{ \AA}$.

2.3 NOAO Mosaic-II imager

We acquired time-resolved photometry from 12 to 18 July 2010 with the Mosaic-II instrument mounted on the Blanco 4-m telescope at the Cerro Tololo Inter-American Observatory. Multiple 120 s exposures of 45 overlapping fields were taken to cover a nine square degree area in the Sloan r' -band containing the GBS X-ray sources reported in Jonker et al. (2011). The order in which the fields were visited was randomized to minimize aliasing caused by regular sampling. Typical seeing conditions during the observations were around 1 arcsec. The last column of Table 1 provides the number of frames containing a detection of the optical counterpart to a GBS source. No photometric data are available for CX522 as the source is unresolved from a bright field star in the Mosaic-II data.

The data were reduced via the NOAO Mosaic Pipeline

which searches and corrects for instrumental artifacts in the image such as cross talk between CCDs. The pipeline applies bias and flat field corrections, and adds a world coordinate system for each image based on USNO-B1 stars in the field. An estimate of the photometric zero-point of the images is also made by comparing the instrumental magnitude of the field star to their USNO B1.0 apparent magnitudes. A detailed explanation of the data reduction procedures can be found in chapter 2 of the NOAO Data Handbook (Shaw 2009).

3 DATA ANALYSIS

3.1 Spectroscopy

Given the uncertain reddening towards the GBS sources and thereby uncertain intrinsic colours, the classification of optical counterparts in this paper was based on the identification of spectral lines and not on the optical continuum measurements. Thus the reduced spectra were normalized by fitting cubic splines to the continuum after masking emission lines, telluric bands and instrumental artifacts. Relevant spectral features were identified and studied. These include late, early or white dwarf type photospheric lines, emission lines and diffuse interstellar bands (DIBs). The normalized spectra of the accreting binaries discussed in this paper are presented in Fig. 1 to 3. For the sake of identification, the rest wavelengths for the following lines are marked in all figures: H β , He I λ 5876, H α and He I λ 6678, 7065 (left panels). In the right panels the markers correspond to the Na I doublet λ 8183, 8195, Ca II λ 8498, P16, Ca II λ 8542, P15, P14, Ca II λ 8662, and P13/12/11/10/9 and 8 (here, P n stands for the Paschen $n - 3$ transition).

Strong features were examined manually with the *splot* task in IRAF obtaining their radial velocity (RV), FWHM and equivalent width (EW). The two first parameters were measured by fitting the line profiles with a Gaussian function, whereas the EW was measured by means of the *splot* keystroke *e*. Table 2 reports the values for the strongest emission lines except for lines which do not have a well-defined profile due to noise and/or telluric contamination problems. Their uncertainties were estimated by looking at the scatter in the values when selecting different wavelength intervals to set the local continuum level. Finally note that all radial velocities provided in the work are heliocentric ones.

3.2 Astrometry

Coordinates for the optical counterparts to the twenty-three GBS sources discussed in the present work are provided in Table 2. Except for CX44, they were obtained from the VI-MOS pre-images after performing an astrometric calibration that delivered a position accurate to RMS < 0.1 arcsec. The position for the optical counterpart to CX44 was derived from Mosaic-II images (see Sec 2.3). Finding charts 20 arcsec \times 20 arcsec wide are shown in the appendix. Observers requiring wider charts can find in Table 1 the necessary details to retrieve from the ESO archive the pre-images for the target of interest.

3.3 Photometry

Photometry was performed using the image subtraction package ISIS (Alard & Lupton 1998, Alard 2000). ISIS uses a reference image which is convolved with a kernel in an effort to match a subsequent image of the same field. This subsequent image is then subtracted from the convolved reference image. Stars which do not vary in magnitude should subtract cleanly, such that the subtracted image is clear of non-variable objects. Therefore, any residual flux is due to an inherent change in brightness of a source. ISIS performs PSF photometry on the subtracted images. The model of the PSF used in each image is build by convolving the PSF model in the reference image with the kernel solution.

In order to save computation time, $104'' \times 104''$ cutouts of the full Mosaic-II images around the position of each X-ray source were taken for processing. The resulting ISIS images were examined by eye to identify variable objects near or at the X-ray positions of the GBS sources. Light curves were then built for these variables and Lomb-Scargle periodograms were used to search for periodicities if enough data points were available. Ellipsoidal modulation is expected in close binaries, in particular in accreting binaries in which the donor star dominates the light curve. We took into account that this type of photometric variability has two maxima and minima in a single orbital cycle and checked periods twice as long as prominent peaks on a periodogram. We also consider both aliases and harmonics, as higher harmonics can sometimes appear at a higher power than the fundamental frequency.

At present, we lack an absolute calibration for these r' -band Mosaic-II data. All apparent magnitudes cited in this paper are a pipeline calibration product (see Sec 2.3). They are to be considered rough estimates and thereby used with caution until secondary standards are established for the Mosaic-II fields. The pipeline zero-point calibration carries an estimated uncertainty of 0.5 mag.

4 RESULTS AND DISCUSSION

4.1 Criteria for the spectroscopic identification of accreting binaries

All counterparts were selected for showing (at least) H α in emission above the continuum. A key motivation of the present work is to report the secure and likely accreting binaries found in this sample and describe the selection criteria used for their identification. We will report on additional candidate counterparts to X-ray sources that showed no H α emission line in their spectrum elsewhere (see e.g. Hynes et al. 2013).

Typically, accreting binaries with hydrogen-rich mass donor stars are unambiguously identified by the presence of broad Hydrogen and Helium emission lines formed in the gas being accreted. Emission from this gas and/or from a white dwarf primary (in the case of CVs) produces a characteristic excess in the optical continuum at blue wavelengths. We have based the identification of accreting binaries on the detection of strong (EW > 18 Å, see below) H α in emission, the Doppler-broadening of the Hydrogen line profiles or the detection of He I λ 6678 emission in the case of observing weak and narrow Hydrogen lines. A search for Carbon, Ni-

trogen and Oxygen emission lines was also performed. Emission from these heavy elements in a spectrum lacking Hydrogen lines is observational evidence for a Carbon-Oxygen white dwarf donor in an ultra-compact X-ray binary (see e.g. Werner et al. 2006, Nelemans et al. 2004, 2006). None were found so far in our sample.

Chromospherically active binaries and stars can be distinguished from qLMXBs and low-accretion rate CVs by the presence of $H\alpha$ emission that does not exceed 15 - 18 Å in EW. This limit is observed in M-type stars (Mohanty & Basri 2003, Covey et al. 2008) and post-common envelope binaries (Bleach et al. 2002), but does not account for the possibility of finding larger EWs during a flare event. In active stars line broadening of the $H\alpha$ profile can be well above the rotational broadening measured in the photospheric lines and reach up to 9 Å ($= 400 \text{ km s}^{-1}$) FWHM in extremely active objects (see e.g. Walter & Basri 1982, Torres et al. 2005). The lack of Helium in emission above the continuum is also a common characteristic of chromospherically active sources. Out of a flare, He I emission above the continuum has been found in a few very active objects (see Bleach et al. 2002 and references therein). From Bleach et al. one can establish that when present in emission, the He I $\lambda\lambda 5876, 6678$ lines do not exceed 3 Å in EW. The He I to $H\alpha$ line ratios are < 0.2 even during flares.

Pre-main sequence stars that host a circumstellar disc (Classic T Tauri stars) may show permitted lines in emission and mimic the optical and X-ray characteristics of reddened CVs and qLMXBs at a low accretion rate state. For instance, they can reach X-ray luminosities of up to $10^{31} \text{ erg s}^{-1}$ (Telleschi et al. 2007), a value typically observed in quiescent black hole LMXBs, and their optical spectra can exhibit broad Hydrogen lines that can appear asymmetric or double-peaked and have EWs of hundreds of Å (e.g. Reipurth et al. 1996, Hamann & Persson 1992, Barrado et al. 2005). Helium lines are often present in the optical spectrum. Fortunately, this young class of objects can be identified on the basis of their association with star formation regions.

4.2 Application to the current sample

Through the analysis of the VIMOS and IMACS spectroscopy we have found optical counterparts to 54 GBS sources. Of the 52 optical counterparts with an $H\alpha$ emission line found in the data, 29 of them are likely chromospherically active objects as they show narrow (unresolved) $H\alpha$ emission with $EW < 3 \text{ Å}$ and a continuum clearly marked by absorption features from a late-type star or binary components¹. Using the SIMBAD database we have not found known star forming regions, star clusters, OB associations or HII regions within one arcmin radius of any of the twenty-three remaining sources. Applying the aforementioned EW limit of 18 Å, fifteen of the 23 sources are classified as accreting binaries. Six of the remaining eight objects (CX70,

CX73, CX93, CX137, CX377 and CX1011) have $H\alpha$ profiles with FWHM ranging 15 – 30 Å. When subtracting in quadrature the instrumental width, they correspond to intrinsic broadenings of 11 – 28 Å ($\sim 500 - 1300 \text{ km s}^{-1}$). Such values are above the 9 Å maximum broadening observed in chromospherically active sources. This indicates that the line profiles in these sources are broadened due to the motion of emitting material in an accretion flow or wind. Finally, the GBS sources CX154 and CX781 qualify as likely accreting binaries on the basis of the presence of He I $\lambda 6678$ in emission with a He I/ $H\alpha$ ratio above the value expected from lines powered by chromospheric activity. Thus, we conclude that all twenty-three sources are most likely accreting binaries.

Of the 23 GBS sources, five (CX44, CX93, CX137, CX154, CX377 and CX1004) show, besides the $H\alpha$ emission from the accretion disc clear evidence of photospheric absorption lines from the donor star. On the other hand, the spectra of CX28, CX63, CX70, CX128, CX142, CX207, CX522, CX784 and CX1011 lack absorption features from such a donor. In these nine systems emission from the accreted gas is the dominant contribution to the total optical light. The other eight objects require other or more observations to establish with certainty the accretion state and the presence of the donor star in the optical spectrum.

4.3 Further constraints on binary parameters from emission line properties

The measured emission line properties provide not only a method to discern accreting binaries from other classes of objects, but also encode a wealth of information on binary parameters such as the system inclination, orbital period, compact object nature or mass accretion rate (see e.g. Warner 1995). In particular the centroid of the line profiles originating in a disc with gas in Keplerian motion will be shifted by the systemic and primary's radial velocities at the time of the observation: $\gamma + K_1 \sin \phi$, where ϕ is the orbital phase, K_1 the radial velocity semi-amplitudes of the primary and γ is the systemic radial velocity. Additional velocities incurred by the gas motion in the accretion disc may be present as well. Furthermore, the line broadening scales with the mass of the compact object, the system inclination and the orbital period as $(M_1/P_{\text{orb}})^{1/3} \sin i$. In this regard, the low intrinsic FWHM of the $H\alpha$ line in CX44 (510 km s^{-1}) suggests a moderate to low inclination for this system and thereby a low $|K_1|$. Thus the large radial velocity offset in the emission lines ($|RV| \sim 200 \text{ km s}^{-1}$) likely reflect a high γ given that the RV component due to the motion of the primary is expected to be low. On this basis, CX44 is a good candidate for an LMXB that experienced a natal kick - CVs in general have low γ (van Paradijs et al. 1996, Ak et al. 2010). The line profiles in CX207 and CX1004 have also significant radial velocity offsets and exhibit the highest line broadening in the sample ($FWHM > 1600 \text{ km s}^{-1}$) in favor of a high inclination for both binaries (both sources are discussed below). However, caution must be taken with this interpretation of the line properties as departures for the simplistic picture of a Keplerian disc are expected and can be dominating the observed RV and FWHM. For instance, complexities in the line profile morphology can result from tidal effects on the disc (Foules et al. 2004) and winds that

¹ These sources will be presented elsewhere once their chromospheric active nature is fully established through further analysis and/or observation. The objects in question are CX25, 29, 47, 57, 74, 124, 126, 161, 251, 294, 321, 325, 381, 393, 409, 450, 469, 502, 634, 642, 712, 820, 852, 858, 881, 895, 1014, 1088 and 1169.

will cause asymmetric profiles. Also, emission originating in regions of the binary system other than the disc can contribute or even dominate the line profile shape and variability. For instance, this is the case in high-magnetic CVs (known as Polars) where the magnetic field of the white dwarf prevents the formation of an accretion disc. Emission lines in these systems can originate from the accretion stream that is directed towards the white dwarf's magnetic poles and from the (irradiated) donor star. As discussed below, a high-magnetic CV is the favoured scenario to explain the emission line properties in CX207.

5 INDIVIDUAL OBJECTS

In what follows, we discuss the spectroscopy and photometry of the twenty-three accreting binaries. We describe remarkable features and provide a characterization of the GBS source on their basis. When useful we will employ the absolute magnitudes and colors of stars as given in Allen's Astrophysical Quantities (Cox 2000) and apply the transformation equations between Johnson-Cousins and SDSS magnitude derived by Jester et al. (2005) and Bilir, Karaali & Tunçel (2005). We will quote from Jonker et al. (2011) the X-ray harness ratio or/and the number of counts detected in the 0.3 - 8 keV band during the discovery observations with *Chandra*. The hardness ratio is defined as $HR = (H-S)/(H+S)$, where S and H are the soft 0.3 - 2.5 keV and hard 2.5- 8 keV band count rates. We provide here counts to 0.5 - 10 keV unabsorbed flux conversion factors of 6.6×10^{-15} and 1.4×10^{-14} erg cm⁻² s⁻¹ count⁻¹. They were obtained using a power-law spectra with index $\Gamma = 2$ modified by a Galactic absorption column density N_H of 10^{21} and 10^{22} cm⁻², respectively. The adoption of this spectral shape for the X-ray sources yields a rough but useful conversion except for soft sources suffering significant reddening in which case the flux will be underestimated by a factor of ~ 10 . Additionally, we give expressions to compute the unabsorbed 0.5 - 10 keV X-ray luminosity as a function of the distance to the source d and the X-ray counts: $L_x(d, N_H = 10^{21}) = 7.9 \times 10^{29} \times \text{counts} \times (\frac{d}{1.0 \text{ kpc}})^2$ and $L_x(d, N_H = 10^{22}) = 1.6 \times 10^{30} \times \text{counts} \times (\frac{d}{1.0 \text{ kpc}})^2$ erg s⁻¹. We will adopt $N_H = 10^{21}$ cm⁻² for objects with bright optical counterparts or lacking strong DIBs and $N_H = 10^{22}$ cm⁻² to faint optical counterparts. The inferred luminosities are below those observed in very-faint persistent neutron star LMXBs (e.g. Armas Padilla et al. 2013) and within the broad range of luminosities observed in CVs (Baskill et al. 2005, Byckling et al. 2010, Reis et al. 2013) and qLMXBs (see e.g. Jonker et al. 2012).

CX28 = CXOGBS J173946.9-271809, a high accretion rate CV

Results based in part on the VIMOS spectrum (Fig. 1) and the Mosaic-II time-resolved photometry suggest that CX28 is a high accretion rate CV. This classification is supported by the detection of the high-excitation emission line He II $\lambda\lambda 4686, 5412$. We refer the reader to Britt et al. (2013) for a full discussion. The absorption lines detected at $\lambda\lambda 8349, 8536, 8659$ in the VIMOS spectrum are caused by

contamination of a late type field star NE from this GBS source. A finding chart for the optical counterpart to CX28 can be found in Britt et al. (2013) as well.

CX39 = CXOGBS J174140.0-271738, an outbursting CV

The VIMOS spectrum of CX39 (Fig. 1) exhibits H α and He I $\lambda\lambda 6678, 7065$ emission with single-peaked asymmetric line profiles of intrinsic FWHM ranging from 700 to 840 km s⁻¹. Note here that the apparent narrow emission features near $\lambda 5900$ are sky-line residuals. Photospheric lines from the donor star are not obvious in the spectrum. The presence of DIBs at $\lambda\lambda 6284, 8620$ is uncertain. The soft X-ray hardness ratio $HR = -0.35 \pm 0.25$ indicates low reddening and thereby a nearby object.

The optical light curve (Fig. 4) shows, what appears to be a brief outburst of 1.2 mag amplitude, rising on the first day of observations and decaying to $r' = 20.2$ over the next 3 days. After that, the counterpart flickers with an RMS scatter of 0.1 mag. We examined the spatial profile of both the optical counterpart spectrum and the spectra of field stars contained in the slit. This together with comparison of the VIMOS pre-images obtained on 31 Mar 2010 and 17 Aug 2010 UT shows that CX39 was not in outburst during the spectroscopic observations.

Recurrent low-amplitude brightenings with fast return to minimum light have been observed in the long-term light curves of dwarf novae (see e.g. Shears et al. 2006) and with lower amplitude in nova-like CVs (Rodriguez-Gil et al. 2012a). In addition, a small number of weak magnetic CVs (Intermediate Polars, IPs) are known to undergo relatively short duration and low amplitude outbursts (see e.g. Ishioka et al. 2002 and references therein).

The lack of stellar features in the quiescent optical spectrum together with this photometric behaviour suggests that CX39 is a dwarf nova or IP with a disc-dominated optical spectrum. The X-ray flux detected with *Chandra* (39 counts) implies $L_x(d, N_H = 10^{21}) = 3.1 \times 10^{31} \times (\frac{d}{1.0 \text{ kpc}})^2$ erg s⁻¹.

CX44 = CXOGBS J17542.8-281809 = AX J1755.7-2818, a qLMXB or a low accretion rate CV

The IMACS spectrum of CX44 (Fig. 1) shows H α and H β in emission. He I $\lambda 5876$ is present while the location of the He I $\lambda 6678$ line fell in a chip gap. The IMACS spectrum also covers the high-excitation line He II $\lambda 4686$, which is not detected. As reported in Sec 4.2, the emission lines exhibit velocity offsets of about -200 km s⁻¹. Moreover, photospheric features from a K-type companion star are visible in the spectrum, the strongest being the molecular bands of the TiO γ' system situated longward of $\lambda 5840$, Ca I $\lambda 6162$ and the blend of Fe I + Ca I at rest wavelength $\lambda 6495$. Gaussian fits to the metal-line profiles yield a -50 km s⁻¹ radial velocity. In the red, the spectrum is dominated by numerous telluric features and shows evidence for absorption from the Ca II $\lambda 8542$ line. There is no obvious detection of the Na I $\lambda 8190$ doublet or Paschen lines (neither in emission nor in absorption). The lack of strong photospheric lines from the donor in this part of the spectrum suggests a significant contribution to the I-band continuum by the accretion disc.

The optical light curve (Fig. 4) shows aperiodic variability with an RMS of 0.05 mag. and with an observed maximum variability of $\Delta r' = r'_{max} - r'_{min} = 0.44$ mag.

CX44 is the unique GBS source within the 50''-radius error circle of AX J1755.7-2818. This ASCA object was found at a 0.7 - 10 keV flux level of 1.2×10^{-12} erg cm⁻² s⁻¹ during a pointing observation on 2 Nov 1999 (Sakano et al. 2002). Thirty-two counts were observed from CX44 with *Chandra* on 4 May 2008. Using an absorbed power law model with $\Gamma = 2$ and N_H ranging $10^{21} - 10^{22}$ cm⁻² we derive an absorbed flux of $(1.7 - 2.5) \times 10^{-13}$ erg cm⁻² s⁻¹ in the 0.7 - 10 keV band. This flux is at least 5 times lower than the value found during the ASCA observation.

Given the lack of strong DIBs in the optical spectrum and the soft X-ray hardness ratio ($HR = -0.19 \pm 0.19$), we expect CX44 to be a nearby (few kpc) binary with a non-evolved donor star. From the apparent optical magnitude ($r' = 18.7$) we obtain a rough estimation of 2 kpc for its distance by assuming a K5 V companion star ($M_{r'} = 7.0$) and by neglecting both the effects of interstellar reddening and veiling from the accretion disc. We also derive $L_x(d, N_H = 10^{21}) \sim 1 \times 10^{32} \times (\frac{d}{2.0 \text{ kpc}})^2$. This X-ray brightness of the source together with, the detection of the donor star and the dominant flickering in the optical light curve suggests that we may have found a nearby low accretion rate CV or a quiescent neutron star LMXB where the accretion disc contributes in a large fraction to the optical light.

CX45 = CXOGBS J173538.5-285251, a CV with an accretion-dominated optical spectrum

The VIMOS spectrum of CX45 (Fig. 1) shows H α and He I $\lambda 6678$ emission. The profiles for both lines are asymmetric and have an intrinsic ≈ 900 km s⁻¹ (FWHM) broadening. The narrow emission features near $\lambda 5900$ are sky-line subtraction residuals. Longward of H α there are no obvious emission lines. There is no clear detection of absorption features from the donor star in the full spectral range covered by VIMOS. The Mosaic-II light curve (Fig. 4) shows flickering with an RMS scatter of 0.39 mag. The amplitude of the observed variability is large: $\Delta r' = 1.5$ mag.

The strong flickering at optical wavelengths together with the apparent lack of photospheric lines from the donor star supports that CX45 is a CV in a state of high mass transfer rate. Alternatively, CX45 could be a low accretion rate CV with the optical spectrum dominated by emission from the accreting flow as for instance observed in short orbital period dwarf novae (see CX128 for more discussion on this type of CVs). The brightness of the X-ray source (32 counts in the *Chandra* detection, $HR = 0.66 \pm 0.24$) yields $L_x(d, N_H = 10^{21}) = 2.5 \times 10^{31} \times (\frac{d}{1.0 \text{ kpc}})^2$.

CX63 = CXOGBS J173411.3-293117, a CV with an accretion-dominated optical spectrum

The optical spectrum of CX63 (Fig. 1) is dominated by the accretion disc, there are no signs of photospheric lines from the donor star. H α and He I $\lambda\lambda 5876, 6678, 7065$ are in emission with intrinsic broadening between $350 - 500$ km s⁻¹ (FWHM). H β is also present and appears to be unresolved. In the red, P8 to P13 emission lines are seen. The intrinsic

broadening for the Paschen lines ranges from 630 to 1000 km s⁻¹ (FWHM).

The optical light curve of CX63 (see Fig. 4) displays events of increased/decreased brightness of up to 0.5 mag from its 21.3 mean magnitude. The RMS scatter in the Mosaic-II photometry is 0.16 mag, while $\Delta r' = 0.85$ mag.

CX63 is bright in X-rays with 26 counts detected with *Chandra* ($HR = 0.16 \pm 0.23$, $L_x(d, N_H = 10^{21}) = 2.1 \times 10^{31} \times (\frac{d}{1.0 \text{ kpc}})^2$). The characteristics of the optical spectrum together with the flickering observed in the light curve support that CX63 is a high accretion rate CV or a low accretion rate CV with an accretion-dominated optical spectrum. The low FWHM values measured from the emission line profiles support a moderate to low inclination system.

CX64 = CXOGBS J173802.7-283126, a CV in a low state of accretion or a CV in the Bulge region

The H α emission line (intrinsic FWHM = 500 ± 10 km s⁻¹) is the only feature detected in the blue part of the VIMOS spectrum of CX64 (Fig. 1). The line profile appears to be redshifted by 200 km s⁻¹. Longward of H α , lines of the Paschen series may be in emission. It is unclear whether DIBs or photospheric lines from the donor star are present due to the noise in the spectrum. The optical counterpart to CX64 is faint with $r' = 22.3$. The Mosaic-II light curve allows us to place an upper limit in the photometric variability of 0.14 mag (RMS).

If H α is originated in the accretion disc, its low intrinsic broadening implies a moderate to low system inclination and thereby K_1 . Given the moderate K_1 and that CVs are expected to have low systemic velocities (see CX207 below for more details), the large velocity offset observed in the line can be explained if CX64 is a bulge CV (accreting at high mass transfer rate). On the other hand, both the radial velocity offset and low line broadening are also consistent with a more nearby CV in a low state. High accretion rate CVs in a low state of mass transfer show narrow emission lines originating in the irradiated donor stars. The radial velocities of these lines reflect therefore the motion of the donor star. The non-detection of He I $\lambda 6678$ in the optical spectrum of CX64 is in support of this possibility as magnetic and nova-like CVs have shown weak He I $\lambda 6678$ or absence of the line during low-state periods (e.g. Kafka et al. 2005, Rodriguez-Gil et al. 2012b). Unfortunately we cannot confirm this scenario as we lack the signal to search for absorption features from the stellar components. On the basis of the X-ray brightness (25 *Chandra* counts, $HR = 0.22 \pm 0.23$) we derive $L_x(d, N_H = 10^{21}) = 2.0 \times 10^{32} \times (\frac{d}{1.0 \text{ kpc}})^2$ erg s⁻¹.

CX70 = CXOGBS J173535.1-295942, a CV with an accretion-dominated optical spectrum

The spectrum of the optical counterpart to CX70 shows the H α and P10 to P15 Hydrogen lines in emission with intrinsic broadening of $\sim 700 - 900$ km s⁻¹ (see Fig. 1 and line parameters in Table 2). The presence of He I $\lambda 6678$ is uncertain as the line position fell on a region of bad rows in the detector. While artifact features make difficult to address the presence of photospheric lines and DIBs in the blue part of the spectrum, it is clear that stellar lines are not present at wavelengths redward of $\lambda 8000$.

The Mosaic-II light curve (Fig. 4) shows significant variability with an RMS of 0.07 mag and $\Delta r' = 0.32$ mag. A Lomb-Scargle periodogram yields a peak at a period of 5.6 hr. However, we find a False Alarm Probability of 7.8% for this period by running Monte Carlo simulations on randomly ordered light curves.

The non-detection of absorption features from the donor star and the photometric flickering suggest a high accretion rate CV or a CV accreting at lower mass transfer rate, but having an accretion-dominated optical spectrum. From the X-ray brightness (24 counts, $HR = 0.63 \pm 0.29$) we obtain $L_x(d, N_H = 10^{21}) = 1.9 \times 10^{31} \times (\frac{d}{1.0 \text{ kpc}})^2 \text{ erg s}^{-1}$.

CX73 = CXOGBS J174447.5-270101

The only emission line detected in the optical spectrum of CX73 (Fig. 1) is H α with an intrinsic FWHM of $730 \pm 20 \text{ km s}^{-1}$. As in CX70 it is difficult to confirm or reject evidence for absorption lines in the blue part of the spectrum. The red part of the data is strongly affected by fringing since the observations were taken before the VIMOS detector upgrade (see Sec. 2.1).

The Mosaic-II light curve (Fig. 4) shows aperiodic variability with an RMS scatter of 0.08 mag and $\Delta r' = 0.19$ mag. This variability supports a significant contribution from the accretion flow to the optical light. Spectroscopic observations (for instance in the I-band) are necessary to further constrain the nature of CX73. An X-ray luminosity of $L_x(d, N_H = 10^{21}) = 1.8 \times 10^{31} \times (\frac{d}{1.0 \text{ kpc}})^2 \text{ erg s}^{-1}$ is derived from the 23 counts ($HR = 0.22 \pm 0.25$) detected with *Chandra*.

CX87 = CXOGBS J173648.1-293639, an outbursting CV

The VIMOS spectrum of the optical counterpart to CX87 can be found in Fig. 2. Due to its low signal-to-noise ratio we only detect H α in emission with FWHM = $1150 \pm 140 \text{ km s}^{-1}$ and EW = $24 \pm 5 \text{ \AA}$. The line profile appears double-peaked with a peak-to-peak velocity separation of $\Delta v = 650 \pm 80 \text{ km s}^{-1}$.

The Mosaic-II light curve (Fig. 4) shows the source declining in brightness by 2.9 mag, reaching minimum brightness ($r' \sim 23$) four days after the first photometric observation. Examination of the VIMOS pre-image taken on 30 Mar 2011 UT and the spatial profile of the optical counterpart in the VIMOS spectrum show that CX87 was most likely in quiescence during the VLT observations.

It is likely that the Mosaic-II photometry was obtained during the final stage of a CV outburst that brightened by more than 2.9 mag at optical wavelengths. This would support a dwarf nova nature for CX87. Alternatively, CX87 could be an outbursting IP. Some IPs have outbursts with a 3-5 mag amplitude and a few days duration. (see e.g. Ishioka et al. 2002). The X-ray flux observed with *Chandra* (21 counts, $HR = 0.31 \pm 0.25$) implies $L_x(d, N_H = 10^{22}) = 3.0 \times 10^{32} \times (\frac{d}{3.0 \text{ kpc}})^2 \text{ erg s}^{-1}$.

CX93 = CX153 = CXOGBS J174444.6-260328, a low accretion rate CV

CX93 is a 0.237 d orbital period CV observed at a low accretion rate state. A complete dynamical study of this source is presented in Ratti et al. (2013a). The VIMOS data for CX93 are analyzed in Ratti's work and therefore we will not discuss them further except for the following erratum: the EWs measured for the H α emission line in the VIMOS spectra are incorrect. Correct values can be found in the present work (Table 2). As a consequence the claim in Ratti et al. of a more active state of accretion at the time of the VIMOS observations must be disregarded. A finding chart for the field of CX93 can also be found in Ratti's work.

CX128 = CXOGBS J174028.3-271136, a likely short orbital period dwarf nova

The emission line spectrum of CX128 (Fig. 2) shows very strong H α and H β emission lines with single-peaked profiles with an intrinsic FWHM of $\sim 1400 \text{ km s}^{-1}$. He I $\lambda\lambda 5876, 6678, 7065$ are also in emission with similar broadening, though they appear double-peaked. He I $\lambda 5876$ is the stronger of these three lines. At longer wavelengths CX128 shows emission lines of the Paschen series. The lines are broad ($1500 - 2100 \text{ km s}^{-1}$ FWHM) with complex (multi-peaked) profiles. Neither photospheric lines nor interstellar bands are detected indicating that light from the accreted material dominates and that the source suffers moderate reddening. The Mosaic-II photometry (Fig. 5) shows flickering of 0.26 mag RMS and $\Delta r' = 0.89$.

The lack in the spectrum of underlying features from the donor can be explained if this GBS source is a high accretion rate (nova-like or magnetic) CV. However, the EWs for the Balmer and Helium lines (Table 2) seem high compared to those observed in nova-like CVs (Rodríguez-Gil et al. 2007a,b; Dhillon et al. 1996). Furthermore, we do not detect emission from He II $\lambda 5412$, a signature that would have been sufficient to confirm the above scenario. An alternative possibility is that CX128 is a dwarf nova CV below the period gap in quiescence at the time of our observations. In this scenario, the contribution from the small donor star to the optical light is veiled by the accretion disc and the spectrum shows only emission lines. Examples of such spectra can be found in the dwarf novae SS UMa, SU UMi and SW UMa (Connon Smith et al. 1997). In particular SW UMa resembles CX128 in the strength of its Balmer lines. *Chandra* detected 15 counts during the discovery observation which yield $L_x(d, N_H = 10^{21}) = 1.2 \times 10^{31} \times (\frac{d}{1.0 \text{ kpc}})^2 \text{ erg s}^{-1}$. If the source is at a distance of $\sim 1 \text{ kpc}$, the X-ray luminosity is consistent with the luminosities found in quiescent dwarf novae (Bycklbycklyng et al. 2010).

CX137 = CXOGBS J175553.2-281633, a low accretion rate CV or qLMXB?

Based on the positional coincidence with the X-ray source, Udalski et al. (2012) identified in their OGLE-IV data the optical counterpart to CX137: a 0.43104 d periodic variable with I=15.11, V-I=1.32. They suggest that the light curve morphology is consistent with an eclipsing binary harbouring a spotted star.

The VIMOS spectrum of the counterpart is dominated by photospheric absorption features (see Fig. 2). Clearly detected is the discontinuity in the continuum at $\lambda 5200$ caused by the Mg *b* triplet and molecular MgH. Also visible are the metallic blends at $\lambda\lambda 6165, 6495$. In the red, the Na I doublet and Ca II triplet are found in absorption. Finally, TiO bands are not detected in the spectral range covered by the spectrum. These spectroscopic characteristics are consistent with those expected from a late G-type/early K-type star (see e.g. Jacoby et al. 1984). However, the EW of the Ca II $\lambda 8542$ line is $\lesssim 2 \text{ \AA}$, lower than the $\gtrsim 3 \text{ \AA}$ observed in stars with the above spectral types (see for instance Fig 23 in Carquillat et al. 1997). Note that the line measurements are not affected of contamination from a partially resolved field star located SE from CX137. The low EWs may indicate an additional source of continuum light veiling the photospheric lines, for instance the accretion disc. On the other hand, the discrepancy in the EWs is not likely to be due to Paschen emission as there is no evidence of other Hydrogen emission lines in the red part of the spectrum. The presence of broad H α in emission also supports an accreting binary nature for CX137. From single Gaussian fitting, we conclude that the H α profile has an intrinsic FWHM and EW larger than 960 km s^{-1} and 6.5 \AA , respectively. While the line position is consistent with its rest wavelength, we measure a $-90 \pm 20 \text{ km s}^{-1}$ radial velocity for the NaD and Ca II photospheric lines found in the red part of the spectrum.

The optical counterpart to CX137 is the brightest in the sample of GBS sources discussed in this paper and it is saturated in most of the Mosaic-II data. As a result, no meaningful variability information is available from the Mosaic-II images. We therefore investigated the publicly available OGLE-IV data sets which at the time of writing consist on a total of 4358 data points in the I-band acquired during the years 2010-2012. Visual inspection of the light curves suggested small changes in brightness and/or morphology during the three years and therefore we analyzed each year separately. We measure a mean I-band magnitude of 15.11, 15.08 and 15.10 (with an RMS of 0.06 mag) and $\Delta r'$ of 0.20, 0.24 and 0.23 mag for 2010, 2011 and 2012, respectively. Periodograms computed for each year have the highest peak centered at $0.21551725(15) \text{ d}$, where the numbers in parentheses quotes the uncertainty in the last digits. This is half of the orbital period since the light curves phase folded on the 0.4 d period show a much less scattered sinusoidal-like modulation than when folded on the 0.2 d periodicity. Thus we confirm the orbital period found by Udalski et al. (2012). The folded light curves (see Fig. 5) show that during 2010 the two maxima and two minima have similar brightness. In contrast, during 2011 and 2012 both minima and maxima occur at different brightness levels. Another characteristic of the light curve is the lack of strong flickering which supports a stellar component as the main contributor to the optical light.

Udalski et al. (2012) interpreted the sinusoidal light curve as due to eclipses in a contact binary where the yearly changes are due to star spots. On the other hand, the light curve morphology can be explained as due to ellipsoidal variability of the companion star in an accreting system observed at low or moderate inclination. In this scenario the long-term variability observed in the ellipsoidal light curve can also be associated to star spots. Other unknown mech-

anisms may also be at play causing the changes in the light curve morphology (see e.g. Thomas et al. 2012, Ratti et al. 2013a).

In an interactive binary the mean density of the Roche lobe-filling donor star can be determined from the orbital period by following Eggleton (1993): $\bar{\rho}(g \text{ cm}^{-3}) \cong 110 P^{-2}(hr) = 1.0$. This indicates that the donor star in CX137 is enlarged compare to G-K main sequence stars since the latter have higher mean densities (the 1.4 g cm^{-3} of our Sun, for instance). We adopt a K5 V companion ($M_V = 7.35$, $M'_r = 6.98, M_I = 5.73$), null reddening and disc contribution to the optical light to derive a crude lower limit to the distance of 0.7 kpc . Additionally, we use the 15 counts detected with *Chandra* to derive an lower limit on the luminosity of $L_x(d, N_H = 10^{21}) > 5.8 \times 10^{30} \times (\frac{d}{0.7 \text{ kpc}})^2 \text{ erg s}^{-1}$.

The detection of photospheric lines and a broad H α emission line in the optical spectrum suggest that CX137 is a CV accreting at low accretion rate or a qLMXB. High resolution spectroscopy will show if CX377 is a single (accreting) or double-lined (contact) binary.

CX142 = CXOGBS J174403.7-312305, a CV with an accretion-dominated optical spectrum

The VIMOS spectrum of CX142 (Fig. 2) shows a source rich in narrow emission lines and lacking photospheric absorption features. DIBs are not observed. At blue wavelengths H α (with intrinsic broadening of $340 \pm 20 \text{ km s}^{-1}$) and He I $\lambda\lambda 5876, 6678, 7065$ lines are visible in emission. In the red, the Ca II triplet at $\lambda\lambda 8542, 8662, 8498$ are prominent emission lines. They are stronger than the nearest Hydrogen lines of the Paschen series - $\text{EW}(\text{Ca II}) / \text{EW}(\text{P14}) \sim 2$.

The Mosaic-II light curve (Fig. 5) shows an RMS scatter of 0.18 mag which is only twice the average statistical error in the photometry. Even though $\Delta r' = 0.6 \text{ mag}$, the source is at the faint edge of what the Blanco observations can detect making it difficult to set strong constraints on the optical variability.

The optical counterpart to CX142 shows spectroscopic characteristics similar to those of a CV accreting at high rate or low accretion rate CV with a major contribution from the disc to the total optical light. The low FWHM values found for all the emission lines (Table 2) supports a system observed at low inclination if the emission-line region is the accretion disc. Given the good quality of the spectrum we speculate that CX142 was observed in outburst, well above the $r' = 22.2$ brightness measured in the Mosaic-II photometry. We lack other objects in the slit to confirm this possibility and thereby confirm a dwarf nova CV nature. We infer $L_x(d, N_H = 10^{21}) = 1.1 \times 10^{31} \times (\frac{d}{1.0 \text{ kpc}})^2 \text{ erg s}^{-1}$ from the 14 counts detected with *Chandra*. Finally, note that strong emission lines from the Ca II infrared triplet have been already reported in CVs. For instance see the spectrum of the dwarf nova system UU Aql near quiescence (Connon Smith et al. 1997) or GW Lib in outburst (van Spaandonk et al. 2010).

CX154 = CXOGBS J173838.7-283539, a low accretion rate CV or qLMXB

Two epochs of spectroscopy separated by about two weeks were acquired, with the second epoch being of higher qual-

ity. This is shown in Fig. 2. $H\alpha$ in emission is observed in both nights, while He I $\lambda 6678$ is only detected in the second observation. The $H\alpha$ emission line is weak ($EW \sim 8 \text{ \AA}$) with an unresolved profile. In the red, the Ca II $\lambda 8542$ appears to be present in absorption with $EW \sim 1.0 \text{ \AA}$ and a radial velocity of $\sim 120 \text{ km s}^{-1}$ in both nights. This line is most certainly a photospheric feature intrinsic to CX154 and not due to contamination from a nearby field star. Finally, from the Mosaic-II data we derive $\Delta r' = 0.5 \text{ mag}$ and an RMS scatter of 0.1 mag .

Based on the likely detection of one of the components of the ionized Calcium triplet, CX154 can be tentatively classified as a low accretion rate CV or qLMXB. The low FWHM shown by $H\alpha$ could be interpreted as originating in a low inclination system if the emission arises from an accretion disc. An alternative scenario is that where the line is produced in the donor star by reprocessing of X-rays from a neutron star or white dwarf primary (e.g. Bassa et al. 2009, Ratti et al. 2012, Rodríguez-Gil et al. 2012). From the 15 counts observed with *Chandra* we estimate $L_x(d, N_H = 10^{21}) = 1.1 \times 10^{31} \times (\frac{d}{1.0 \text{ kpc}})^2 \text{ erg s}^{-1}$.

CX207 = CXOGBS J174625.3-263133, a likely Polar

Spectra of the optical counterpart to CX207 were obtained in two nights separated one month. In both nights, the spectrum is dominated by strong $H\alpha$ in emission ($EV > 80 \text{ \AA}$). This line is remarkable for being single-peaked despite its broadening ($FWHM = 1500 - 1600 \text{ km s}^{-1}$) and because it presents a large radial velocity offset ($|RV| > 350 \text{ km s}^{-1}$) with respect to its rest wavelength. Weaker He I and Paschen emission is also detected in the spectrum. $H\alpha$ and some of the other features are consistent with having two-component line profiles. The two epochs of spectroscopy show clear variability in the line profiles, in particular their central wavelengths (see Table 2).

The optical light curve for CX207 (Fig. 5) shows an eclipse of a depth more than 3 mag at HJD 2455389.590991 and a possible second eclipse in progress at HJD 2455386.633003 when the source is observed 1 mag fainter than its mean brightness. Outside these two events, the Mosaic-II data has $\Delta r' = 0.7$ and aperiodic variability with an RMS of 0.2 mag .

The optical spectrum of CX207 resembles that of the neutron star X-ray binary Circinus X-1 (Mignani 1997, Johnson et al. 2001, Jonker et al. 2007) or the black-hole transient V4641 Sagittari (Lindström et al. 2005). In this case the large broadening, large radial velocity offset and variability may be due in part to an outflow in an active X-ray binary harbouring a compact primary and a early-type companion. This model for CX207 requires the X-ray binary to be at a large distance and suffer significant reddening in order to explain the faintness of the X-ray and optical counterparts (11 *Chandra* counts equivalent to $L_x(d, N_H = 10^{21}) = 8.7 \times 10^{30} \times (\frac{d}{1.0 \text{ kpc}})^2 \text{ erg s}^{-1}$, $r' = 21.1$). However, the optical spectrum lacks evidence for strong DIBs ruling out this scenario and favours the possibility that CX207 is a nearby CV. In this regard, broad single peaked emission lines are typically observed in nova-like variables. In this class of high-accretion rate CVs even

eclipsing systems do not show a double-peaked profile. The optical spectra in nova-like CVs can show emission lines that reach profile broadenings of values similar to that observed in CX207 (see e.g. Rodríguez-Gil et al. 2007a,b; Dhillon et al. 1992). In this scenario the large radial velocity offset observed in CX207 will have to reflect a combination of a large systemic velocity and K_1 . Alternatively, CX207 may be a member of the magnetic (Polar) class of CVs. These systems can exhibit emission lines with similar line morphology and large EWs as observed in the GBS source. In Polars the line profile is composed of (at least) a narrow and a broad component, the former originating in the irradiated donor star. These components can exhibit radial velocities comparable or larger than those measured here - see for instance the eclipsing Polars EXO 033319 - 2554.2 (Allen et al. 1998), MN Hya (Ramsay & Wheatley 1998) and the non-eclipsing system ET Can (Williams et al. 2013). Given that the observed systemic radial velocities in nova-like CVs do not go above $\sim 200 \text{ km s}^{-1}$ (Ak et al. 2010), the magnetic CV scenario seems more likely as it does not require of such unusual high γ to explain the radial velocities of the emission lines in CX207.

CX377 = CXOGBS J174316.5-274537, a likely low accretion rate CV or qLMXB

Two epochs of spectroscopy separated by nearly two months were obtained with VIMOS. In Fig 2. we show the spectrum obtained on 23 Jul 2011 UT with the slit oriented such to avoid spatial blending with the nearby field stars. $H\alpha$ is unambiguously detected in emission. Unfortunately, instrumental artifacts are also apparent in the blue part of the spectra. This makes it difficult to address the presence/absence of stellar features and interstellar bands at wavelengths shorter than $H\alpha$. To achieve the detection of photospheric lines we extracted and studied the spectra of field stars in the CX377 slit. In this way we confirm the non detection of the metallic blends at $\lambda\lambda 6165, 6495$ which are strong features in the spectra of late-type stars. We cannot establish the presence of He I emission at $\lambda 6678$. In the red, the spectrum reveals the absorption lines from the Ca II infrared triplet. On the other hand, neither the Na I double nor the P14 $\lambda 8598$ line or TiO bands appear to be present at the time of the observations. These spectroscopic characteristics suggest a late F-type/early G-type donor star in CX377 (see e.g. Jacoby et al. 1984, Zhou 1991, Munari & Tomasella 1999). We measure for the Ca II $\lambda 8542$ line an EW of $\sim 1.5 \text{ \AA}$, lower than the values observed in F/G of any luminosity class (Jones et al. 1984, Zhou 1991). As in CX137 this discrepancy can be due to veiling of the lines by the accretion disc continuum emission. Disc veiling could also explain the non detection of the metallic lines described above.

During the two epochs of spectroscopy the profile of the $H\alpha$ emission line is intrinsically broadened by $\sim 1200 \text{ km s}^{-1}$ (FWHM) and asymmetrically double-peaked with the blue peak being stronger than the red peak. The double-peak separation is $\Delta v = 610 \pm 20 \text{ km s}^{-1}$ and $\Delta v = 720 \pm 30 \text{ km s}^{-1}$ during the first and second epoch, respectively. Given the asymmetry in the line profiles, a better estimation of the line center than that obtained from a Gaussian fit (Table 2) is provided by the centroid of the line derived from the

emission line peaks. We measure in this way radial velocities of $70 \pm 20 \text{ km s}^{-1}$ and $60 \pm 30 \text{ km s}^{-1}$ for the first and second epoch, respectively. Both values are consistent within the errors. On the other hand, we derive from the Ca II triplet radial velocities of $80 \pm 6 \text{ km s}^{-1}$ and $90 \pm 10 \text{ km s}^{-1}$ for epoch 1 and 2, respectively. These velocities are consistent with those measured from H α . Note here that the emission line is weak ($EW \sim 7 \text{ \AA}$) and thereby its double-peak morphology may be caused by the underlying photospheric H α .

The VIMOS spectra also show the $\lambda 8620$ DIB with an $EW = 0.7 \pm 0.1 \text{ \AA}$. We derive $E(B-V) = 1.9 \pm 0.2$ according to the relation between reddening and EW for this interstellar band (Munari 2000). This value is equal to the 1.9 ± 0.3 mag derived from the reddening maps of the Galactic bulge (Gonzalez et al. 2012; these maps have a spatial resolution of $2 \times 2 \text{ arcmin}^2$ resolution).

The Mosaic-II light curve of CX377 (Fig 5) shows photometric variability with an RMS scatter of 0.05 mag and $\Delta r' = 0.22$ mag. There is no evidence for a periodic modulation.

The detection of the donor star in the VIMOS spectrum, the H α profile broadening and the high reddening towards the source suggest that CX377 is a (bulge) low accretion rate CV observed at a moderate inclination or a bulge qLMXB. Using the relationship of Bohlin et al. (1978) $N_H = 5.8 \times 10^{21} \times E(B-V) \text{ cm}^{-2}$ and adopting as before an absorbed power-law spectrum with index $\Gamma = 2$, we derive from the detect 7 *Chandra* counts an unabsorbed flux of $1.0 \times 10^{-13} \text{ erg cm}^{-2} \text{ s}^{-1}$ (0.5 - 10 keV) and a luminosity of $L_x(d, N_H = 1.1 \times 10^{22}) = 7.6 \times 10^{32} \times (\frac{d}{8.0 \text{ kpc}})^2 \text{ erg s}^{-1}$.

CX446 = CXOGBS J174627.1-254952, a high inclination CV or qLMXB

The spectrum of the optical counterpart to CX446 can be found in Fig. 3. Due to its low signal-to-noise ratio we only detect strong H α in emission with $EW = 50 \pm 4 \text{ \AA}$. The line profile appears single-peaked despite its large intrinsic broadening ($FWHM = 2200 \pm 50 \text{ km s}^{-1}$). This appearance may be caused both by noise and/or the presence of a narrow emission line component filling-in the region between the two peaks. The large line broadening is suggestive of a high inclination system. In fact, the Mosaic-II light curve (Fig. 5) shows an eclipse-like event at HJD 2455387.824233 with a 0.4 mag depth with respect to a mean 21.16 r' band magnitude. Our photometric sampling does not allow us to set constraints on the duration of this event. Other decreases in brightness observed in the light curve are consistent either with photometric variability and/or another eclipses. We performed a periodicity analysis of this light curve but this yielded no significant period.

In summary, the broadening of the line and the eclipse-like event observed in the light curve suggest a high inclination (eclipsing) CV or qLMXB nature for CX446. From the 6 counts detected by *Chandra* we estimate $L_x(d, N_H = 10^{21}) = 4.7 \times 10^{30} \times (\frac{d}{1.0 \text{ kpc}})^2 \text{ erg s}^{-1}$.

CX522 = CXOGBS J175432.5-282918, a CV with an accretion-dominated optical spectrum

The optical counterpart to this GBS source was misidentified in Udalski et al. (2012) with a close bright field star. The

coordinates for the correct optical counterpart to CX522 can be found in Table 2. The VIMOS spectrum (Fig. 3) shows , H β and He I $\lambda\lambda 5876, 6678, 7065$ with some evidence for Paschen emission in the red part of the spectrum. H α is moderately broad with $850 \pm 10 \text{ km s}^{-1}$ FWHM. Neither photospheric lines from the donor star nor strong DIBs are detected.

The optical counterpart to CX522 is too close to the bright field star mentioned above to allow for a reliable photometric study on the Mosaic-II data. From the VIMOS pre-images obtained on 8 Apr 2011 UT we derive $R \sim 22$ by performing differential photometry respect to the USNO B1.0 object 0615-0617155 ($R1 = 18.68$). On the other hand, examination of the spatial profile of both the optical counterpart spectrum and the spectrum of a field star partially contained in the slit suggests that CX522 may have been brighter at the time of the spectroscopic observations .

On the basis of the spectroscopic characteristics described above, CX522 is a high accretion rate CV or a low accretion rate CVV with an accretion-dominated optical continuum. The 5 counts detected with *Chandra* imply $L_x(d, N_H = 10^{21}) = 4 \times 10^{30} \times (\frac{d}{1.0 \text{ kpc}})^2 \text{ erg s}^{-1}$.

CX772 = CXOGBS J174405.0-263159

Only broad H α in emission with an intrinsic FWHM of $900 \pm 180 \text{ km s}^{-1}$ is apparent in the VIMOS spectrum (Fig. 3). On the other hand, it is not possible to address the presence of line features in the red part of the spectrum given that the spectrum is affected by fringing - the observations were taken before the upgrade of the VIMOS detectors (see Sec. 2.1).

We measure $\Delta r' = 1.5$ and an RMS scatter of 0.28 mag for the light curve of CX772 (see Fig. 6). However, the brightness of the optical counterpart ($r' = 22.2$) is at the faint end of the range of detected objects in the Mosaic-II data. Thus the photometry has on average a large uncertainty of 0.18 mag.

With the current data we cannot establish the nature of CX207 further than it is a CV or a qLMXB. The 4 counts detected with *Chandra* yield $L_x(d, N_H = 10^{21}) = 3.2 \times 10^{31} \times (\frac{d}{1.0 \text{ kpc}})^2 \text{ erg s}^{-1}$.

CX781 = CXOGBS J174311.1-271621, a CV with an accretion-dominated optical spectrum

The VIMOS spectrum of CX781 (Fig. 3) exhibits H α and He I $\lambda 6678$ emission with unresolved line profiles. The H α line profile is weak with $EW = 5.0 \pm 0.2 \text{ \AA}$. Instrumental artifacts are evident in the blue part of the spectrum making difficult to identify stellar features and interstellar bands at wavelengths shorter than H α . In the red part of the spectrum (right panel) absorption lines from the donor star are not detected, in particular, there is no evidence of the CaII triplet in absorption. Only H γ $\lambda 9229$ (P11) seems to be present, but in emission.

The Mosaic-II light curve for the optical counterpart to CX781 (Fig. 6) exhibits clear variability: the source brightness decreases by 0.25 mag four days after the start of the observations to return slowly to full brightness of $r' = 17.9$ mag approximately four days later. Long-term erratic variability usually observed in accreting binaries can explain this

behaviour. There is also variability at shorter time scales (flickering) of 0.05 mag amplitude. We derive $\Delta r' = 0.28$ mag and RMS of 0.09 mag from the whole light curve.

The lack of photospheric features in the VIMOS spectrum, the detection of flickering together with possible erratic long-term photometric variability support both a high accretion rate CV nature or a low accretion rate CV where the accretion flow is the dominant source of optical continuum - a short orbital period IP or dwarf nova in quiescence for instance. The narrow and weak H α emission line is arising either in the disc of a low inclination binary or in the irradiated hemisphere of the donor star. We estimate $L_x(d, N_H = 10^{22}) = 3.2 \times 10^{30} \times (\frac{d}{1.0 \text{ kpc}})^2 \text{ erg s}^{-1}$. from the 4 counts detected with *Chandra*.

CX794 = CXOGBS J174142.3-275829, an eclipsing nova-like

Udalski et al. (2012) reported an I=19.4 optical counterpart to CX794 and found in the OGLE light curve a possible 0.11786 d period together with evidence for eclipses. Dimming events of up to 2 mag are apparent in the Mosaic-II photometry (Fig. 6) as well as in the public OGLE light curve. A Lomb-Scargle periodogram analysis of our data shows a 0.1179 d period with another peak at 0.1052 d, adding weight to the period reported by Udalski et al. (2012). The long (~ 2 years) interval spanned by the OGLE observations allows us to assess the eclipsing nature of CX794 and establish its orbital period by using an O-C curve analysis. For this we have taken the minimum brightness in the OGLE light curve to be the event closest to or at the time of a mid-eclipse. This yields the following ephemeris: $T_{\text{mid-eclipse}} = \text{HJD } 2455768.57874 + 0.11786 \times E$. Next the times for eleven events with a > 0.6 mag drop in brightness were identified in both the OGLE and Mosaic-II data. The O-C curve (not shown) displays < 0.1 cycles offsets between these times and the eclipse times derived from the ephemeris. The same analysis shows that the periodicities found in the Mosaic-II data gave larger residuals. Fig. 6 shows the Mosaic-II light curve folded on the above ephemeris.

Our optical spectrum (Fig. 3) shows H α , H β and He I $\lambda\lambda 5876, 6678, 7065$ lines in emission. The FWHM of H α (1050 km s^{-1}) is on the low side for a high-inclination system. Furthermore, the line profiles of both lines are single-peaked. Lines from the Paschen series are also detected in emission with P9 being the strongest. On the other hand, there is no evidence for absorption features from the donor star or the interstellar medium.

These above properties suggest that CX794 is a high accretion rate CV within the 2-3 hr period gap and with spectroscopic similarities to the SW Sextantis nova-like variables. We derive $L_x(d, N_H = 1.1 \times 10^{21}) = 3.2 \times 10^{30} \times (\frac{d}{1.0 \text{ kpc}})^2 \text{ erg s}^{-1}$ from the 4 *Chandra* counts. At present we lack an infrared counterpart to obtain a reliable constraint on the distance towards the source by using the method by Knigge (2006).

CX1004 = CXOGBS J174623.5-310550, a low accretion rate eclipsing CV or qLMXB

The most remarkable feature in the spectrum of CX1004 (Fig. 3) is a broad double-peaked H α emission line with FWHM = $2120 \pm 20 \text{ km s}^{-1}$ and a peak-to-peak velocity separation of $\Delta v = 1170 \pm 10 \text{ km s}^{-1}$. This is the single emission line detected in the spectrum. The centroid of the H α line profile measured using the red and blue peak positions yields a radial velocity of $-170 \pm 20 \text{ km s}^{-1}$, slightly lower than the value obtained by fitting a single Gaussian to the line profile (Table 2). Absorption bands are prominent in the spectral range 5850 – 7350 Å and are caused by the TiO α, β, γ and γ' band systems (see e.g. Coelbo et al. 2005 for their identification in a broad-band spectrum). Redward of 8000 Å the δ and ϵ systems are not detected. In this region the Na I doublet at $\lambda\lambda 8183, 8195$ is in absorption together with the Ca II and Hydrogen atomic lines. No interstellar features are found, except perhaps for the NaD doublet at $\lambda\lambda 5890, 5896$ unresolved from their stellar counterparts. We measure a radial velocity of $-170 \pm 20 \text{ km s}^{-1}$ from fits to the metallic lines in the red part of the spectrum. This value is in agreement with the radial velocity obtained from the H α emission line.

On the other hand, the Mosaic-II light curve (Fig. 6) does not exhibit significant photometric variability for this source in 35 observations. The RMS scatter and $\Delta r'$ in the photometry is 0.04 mag and 0.17 mag, respectively.

The large FWHM and peak-to-peak velocity separation in the H α profile in CX1004 is similar to that observed in eclipsing dwarf novae CVs in quiescence or qLMXBs harboring a black-hole. Examples are OY Car ($P_{\text{orb}}=1.51 \text{ hr}$, $\Delta v = 1160 \text{ km s}^{-1}$; Schoembs & Hartmann 1983), U Gem ($P_{\text{orb}}=4.22 \text{ hr}$, $\Delta v = 920 \text{ km s}^{-1}$; Echevarria et al. 2007, Naylor et al. 2005), XTE J1118+480 ($P_{\text{orb}}=4.08 \text{ hr}$, $\Delta v = 1800 \text{ km s}^{-1}$; Torres et al. 2004) and A0620-00 ($P_{\text{orb}}=7.68 \text{ hr}$, $\Delta v = 1270 \text{ km s}^{-1}$; Marsh et al. 1994).

As shown above, the detection of photospheric lines and the large broadening of the H α emission line are properties that suggest that CX1004 is an eclipsing CV accreting at low accretion rate or a high inclination qLMXB with a black hole primary. However, the lack of significant photometric variability is difficult to explain as we would expect to see eclipses, an ellipsoidal modulation and/or flickering. Finally, the lack of DIBs suggests a nearby source for which we derive from the 3 *Chandra* counts an X-ray luminosity of $L_x(d, N_H = 10^{21}) = 2.4 \times 10^{31} \times (\frac{d}{1.0 \text{ kpc}})^2 \text{ erg s}^{-1}$. As a reference an M2 V ($M'_r = 9.14$) unreddened star with the same apparent magnitude as CX1004 will be at a 2.1 kpc distance.

CX1011 = CXOGBS J174604.7-311722, a nova-like variable

A strong feature in the VIMOS and IMACS spectrum (Fig. 3 and 7) is H α with a narrow and weak emission line profile contained within a broad absorption component. Redward of H α , He I $\lambda 6678$ is in emission as well as several Paschen lines with P9 being the strongest of them. In addition to the saturated interstellar NaD doublet, DIBs at $\lambda 5780$ and $\lambda 6284$ are prominent with EWs of $0.40 \pm 0.03 \text{ \AA}$ and $1.28 \pm 0.05 \text{ \AA}$, respectively. Photospheric lines from the donor star

are not detected, in particular, there is no evidence of the CaII triplet in absorption or emission.

The spectral resolution and blue coverage provided by the IMACS observation (Fig. 7) allows us to measure an intrinsic FWHM of $578 \pm 2 \text{ km s}^{-1}$ for H α and we find that the other Balmer lines are composed by a broad absorption component filled-in with core emission. We have measured the full-width zero intensity (FWZI) of the absorption components to be 7522 ± 555 , 4964 ± 898 and $4593 \pm 950 \text{ km s}^{-1}$ for H β , H γ and H δ , respectively. The large uncertainties are due to the difficulty of defining the continuum. Broad HeII $\lambda 4686$ and the CIII/NIII Bowen blend near $\lambda 4648$ are obvious in the IMACS spectrum. We also detect HeI $\lambda 4471$ with emission and absorption components as observed for the Balmer lines.

This source is near the saturation limit of the Mosaic-II data. There are 28 observations which do not saturate. As shown in Fig. 6, the photometry is characterized by low-amplitude flickering with an RMS of 0.01 mag and $\Delta r' = 0.04$. This variability is not significantly correlated with the seeing, which suggests it is real and not a product of the non-linear CCD response at high count rates.

We derive an $E(B-V) = 0.8$ mag from the calibration between reddening and the EW for the $\lambda 5780$ DIB (Herbig 1993). This value is smaller than the 1.6 ± 0.2 mag obtained from the reddening maps of the Galactic bulge (Gonzalez et al. 2012). Using $N_H = 5.8 \times 10^{21} \times E(B-V) \text{ cm}^{-2}$ (Bohlin et al. 1978) and an absorbed power-law spectrum with photon index $\Gamma = 2$, we calculate from the detected 3 *Chandra* counts an unabsorbed flux of $5.7 \times 10^{-14} \text{ erg cm}^{-2} \text{ s}^{-1}$ (0.5 - 10 keV) and X-ray luminosity of $L_x(d, N_H = 4.6 \times 10^{21}) = 6.1 \times 10^{31} \times (\frac{d}{3.0 \text{ kpc}})^2 \text{ erg s}^{-1}$.

The presence of high excitation emission lines and broad absorption lines of HI and HeI partially filled-in by emission cores is frequently observed in nova-like variables (non magnetic CVs in a state of high accretion rate). The narrow emission cores observed in CX1011 suggests a low-inclination system. However, we cannot exclude an origin for the emission in the irradiated donor star or hot spot instead of the disc as observed in the nova-like IX Vel (Beuermann & Thomas 1990). The optical spectrum of CX1011 resembles that of IX Vel except that in our spectrum we do not detect HeI $\lambda 4922$ in emission and the Bowen blend appears stronger than the HeII $\lambda 4686$ line.

6 CONCLUSIONS AND REMARKS

In this paper and in Britt et al. (2013) we have utilized optical spectroscopy to identify the emission line optical counterparts to twenty eight GBS sources and to classify them as accreting binaries. To derive sample of accreting binaries from the optical counterparts to GBS sources as clean as possible of unrelated objects, we have adopted three discriminators, viz. H α in emission with i) $EW > 18 \text{ \AA}$, ii) $FWHM > 400 \text{ km s}^{-1}$ and/or the presence of HeI $\lambda \lambda 5876, 6678$ emission with $EW > 3 \text{ \AA}$ and $EW(\text{He I})/EW(\text{H}\alpha) > 0.2$. Such a selection towards strong H α emitters permits to derive a sample weakly or not contaminated by chromospherically active stars/binaries which are expected to represent $\sim 40\%$ of the X-ray sources found in the GBS area (Jonker et al. 2011). In fact we have identified with VIMOS a large num-

ber of optical counterparts to GBS sources that show spectra characteristic of this type of sources. A disadvantage of using this approach is that accreting binaries with an emission line spectrum not fulfilling any of the above criteria will be missed. Furthermore, a selection based only on the detection of objects with emission lines, blue colours or/and a composed disc – donor spectra will neglect sources in quiescence with spectra fully or mostly dominated by the donor star. For instance, the black hole LMXBs GRO J1655-40 (Orosz et al. 1997; Shahbaz et al. 1997), 4U 1543-47 (Orosz et al. 1998) and SAX J1819.3-2525² (Orosz et al. 1998) would have been overlooked since during quiescence the emission lines may become apparent as residual features only after subtracting the donor star spectrum. The same selection caveat can affect systems harboring less massive primaries. This is the case of IGRJ19308+053 (Ratti et al. 2013b) where light from the F-type companion dominates over both accretion disc and white dwarf emission. Another interesting example is the millisecond radio pulsar FIRST J102347.6+003841 (Thorstensen & Armstrong 2005, Wang et al. 2009) where occasionally only photospheric features from the G-type dwarf donor are detected during quiescence. While low in number, such objects are of interest for two reasons: first, A and F donors are visible at larger distances and reddening than cooler companions. Second, their optical and infrared counterparts are partially or totally free of variable emission from the accretion disc. As a consequence inclination and distance measurements become less dependent on uncertainties in the disc contribution to the total light. The selection effect also applies to LMXBs in hierarchical triple systems in which the main source of optical light during quiescence is the star orbiting around the inner LMXB. Considering only the two confirmed triple systems among the current sample of recycled millisecond pulsars, we expect a $\sim 10\%$ of the LMXBs to be triple system.

In order to increase the chances of finding accreting binaries in sources with no or only weak signs of on-going accretion in their optical spectra, spectroscopic surveys should also employ radial velocity measurements. Stellar-like objects with high radial velocities (or proper motions) should be re-observed to confirm if they are binaries. The reason for this is that, except for runaway stars, field stars in the direction of the bulge should show only small radial motions with respect to the Sun. A radial velocity search for accreting binaries will be sensitive to LMXBs with cool (G to M-type) donors and black hole LMXBs with cool (G to M) and hot (A to F-type) donors since in these cases $q \lesssim 1$ and thereby $K_2 \gtrsim 100 \text{ km s}^{-1}$ for orbital periods less than a day. Detection of neutron star LMXBs and CVs with hot

² For the sake of completeness and comparison, we provide orbital parameters for several sources examined in this section. GRO J1655-40: $P_{orb}=2.62 \text{ d}$, $\gamma = -142 \text{ km s}^{-1}$, $K_2 = 228 \text{ km s}^{-1}$, $q=0.33$; F3-6 IV companion. 4U 1543-47: $P_{orb}=1.12 \text{ d}$, $\gamma = -82 \text{ km s}^{-1}$, $K_2 = 124 \text{ km s}^{-1}$, A2 V companion. SAX J1819.3-2525: $P_{orb}=2.82 \text{ d}$, $\gamma = 107 \text{ km s}^{-1}$, $K_2 = 211 \text{ km s}^{-1}$, $q=0.67$, B-type companion. FIRST J102347.6+0038: $P_{orb}=4.75 \text{ hr}$, $\gamma = 1 \text{ km s}^{-1}$, $K_2 = 268 \text{ km s}^{-1}$, mid-G V companion. IGRJ19308+053: $P_{orb}=0.61 \text{ d}$, $\gamma = -18 \text{ km s}^{-1}$, $K_2 = 91 \text{ km s}^{-1}$, $q=1.78$, F-type companion. Cyg X-2; $P_{orb}=9.84 \text{ d}$, $\gamma = -210 \text{ km s}^{-1}$, $K_2 = 86 \text{ km s}^{-1}$, $q=0.34$ A9 III companion. Cen X-4: $P_{orb}=15.1 \text{ hr}$, $\gamma = 184 \text{ km s}^{-1}$, $K_2 = 150 \text{ km s}^{-1}$, $q=0.17$ K3-5 V companion.

donors in a single radial velocity measurement is more unlikely since $q \gtrsim 1$ and $K_2 \lesssim 100 \text{ km s}^{-1}$ (however, see Ratti et al. 2013b). Furthermore, some neutron star LMXBs may have received a significant natal kick that may result in a high systemic radial velocity for the system. Examples of systems with a high γ are Cyg X-2 (Casares et al. 1998, Kolb et al. 2000) and Cen X-4 (Torres et al. 2002, González Hernández et al. 2005). Accreting binaries in the Bulge may also have a high radial velocity component caused by the kinematics in this region. Bulge members can be identified by the presence of strong DIBs in their optical spectra. The strengths in many of these features correlate well with the extinction towards the source and thereby they can be used together with 2D/3D extinctions maps of the GBS areas (e.g. Gonzalez et al. 2012, Chen et al. 2013). The GBS, with a selection of sources based on their X-ray detection, a spectroscopic search accounting for radial velocities and a photometric scrutiny to identify ellipsoidal variables, will allow us to investigate the frequency and nature of accreting binaries lacking signs for accretion activity in their optical spectra.

APPENDIX A: FINDING CHARTS

Finding charts (only on-line) for the optical counterparts to 20 of the 23 accreting binaries presented in this paper. North is up and East is to the left. The charts are 20 arcsec square with the optical counterpart in the center. The images have been created by using R-band images obtained with VIMOS (except for CX44 for which Mosaic-II r' -band imaging was used). Finders for CX28 and CX93 can be found in Britt et al. (2013) and Ratti et al. (2012), respectively.

ACKNOWLEDGMENTS

We are thankful to Marina Rejkuba (ESO) for supporting our service mode observations with VIMOS. We are grateful to Eva Ratti, Oliwia Madej and Marianne Heida and for helping in the preparation of the VIMOS masks. We also thank Victoria Gabb and Monique Villar for assistance with Mosaic-II data analysis and Lauren Gossen for assistance at the Blanco telescope. PGJ acknowledges support from a VIDI grant from the Netherlands Organisation for Scientific Research. DS acknowledges support from STFC through an Advanced Fellowship (PP/D005914/1) as well as grant ST/I001719/1 RIH, CTB and CBJ acknowledge support from the National Science Foundation under Grant No. AST-0908789.

REFERENCES

- Ak, T., Bilir, S., Ak, S., Coşkunoglu, K. B., & Eker, Z. 2010, *Nat*, 15, 491
- Alard, C. & Lupton, R.H., 1998, *ApJ*, 503, 325
- Alard, C. 2000, *A&AS*, 144, 363
- Allen, R. G., Berriman, G., Smith, P. S., & Schmidt, G. D. 1989, *ApJ*, 347, 426
- Andrillat, Y., Jaschek, C., & Jaschek, M. 1995, *A&AS*, 112, 475
- Armas Padilla, M., Degenaar, N., & Wijnands, R. 2013, *MNRAS*, 434, 1586
- Baskill, D. S., Wheatley, P. J., & Osborne, J. P. 2005, *MNRAS*, 357, 626
- Bassa, C. G., Jonker, P. G., Steeghs, D., & Torres, M. A. P. 2009, *MNRAS*, 399, 2055
- Barrado y Navascués, D., & Martín, E. L. 2003, *AJ*, 126, 2997
- Beuermann, K., & Thomas, H.-C. 1990, *A&A*, 230, 326
- Bigelow, B. C., & Dressler, A. M. 2003, *Proc. SPIE*, 4841, 1727
- Bilir, S., Karaali, S., & Tunçel, S. 2005, *Astronomische Nachrichten*, 326, 321
- Bleach, J. N., Wood, J. H., Smalley, B., & Catalán, M. S. 2002, *MNRAS*, 335, 593
- Bottini, D., Garilli, B., Maccagni, D., et al. 2005, *PASP*, 117, 996
- Bohlin, R. C., Savage, B. D., & Drake, J. F. 1978, *ApJ*, 224, 132
- Britt, C. T., Torres, M. A. P., Hynes, R. I., et al. 2013, *ApJ*, 769, 120
- Byckling, K., Mukai, K., Thorstensen, J. R., & Osborne, J. P. 2010, *MNRAS*, 408, 2298
- Carquillat, M. J., Jaschek, C., Jaschek, M., & Ginestet, N. 1997, *A&AS*, 123, 5
- Casares, J., Charles, P. A., & Kuulkers, E. 1998, *ApJ*, 493, L39
- Coelho, P., Barbuy, B., Meléndez, J., Schiavon, R. P., & Castilho, B. V. 2005, *A&A*, 443, 735
- Connon Smith, R., Sarna, M. J., Catalan, M. S., & Jones, D. H. P. 1997, *MNRAS*, 287, 271
- Covey, K. R., Agüeros, M. A., Green, P. J., et al. 2008, *ApJS*, 178, 339
- Cox, A. N. 2000, *Allen's Astrophysical Quantities*, Springer (AIP Press), New York
- Chen, B. Q., Schultheis, M., Jiang, B. W., et al. 2013, *A&A*, 550, A42
- Dhillon, V. S. 1996, *IAU Colloq. 158: Cataclysmic Variables and Related Objects*, 208, 3
- Echevarría, J., de la Fuente, E., & Costero, R. 2007, *AJ*, 134, 262
- Eggleton, P. P. 1983, *ApJ*, 268, 368
- Foulkes, S. B., Haswell, C. A., Murray, J. R., & Rolfe, D. J. 2004, *MNRAS*, 349, 1179
- González Hernández, J. I., Rebolo, R., Peñarrubia, J., Casares, J., & Israelian, G. 2005, *A&A*, 435, 1185
- Gonzalez, O. A., Rejkuba, M., Zoccali, M., et al. 2012, *A&A*, 543, A13
- Greiss, S., Steeghs, D., Maccarone, T., et al. 2011a, *The Astronomer's Telegram*, 3562, 1
- Greiss, S., Steeghs, D., Maccarone, T., et al. 2011b, *The Astronomer's Telegram*, 3688, 1
- Greiss, S., et al. 2013, submitted to *MNRAS*
- Hamann, F., & Persson, S. E. 1992, *ApJS*, 82, 247
- Herbig, G. H. 1993, *ApJ*, 407, 142
- Hynes, R. I., Britt, C. T., Jonker, P. G., Wijnands, R., & Greiss, S. 2012b, *The Astronomer's Telegram*, 4417, 1
- Hynes, R. I., Wright, N. J., Maccarone, T. J., et al. 2012a, *ApJ*, 761, 162
- Hynes, R. I., et al. 2013 *ApJ*, submitted to *ApJ*
- Ishioaka, R., Kato, T., Uemura, M., et al. 2002, *PASJ*, 54, 581
- Izzo, C., Kornweibel, N., McKay, D., et al. 2004, *The Messenger*, 117, 33

- Jacoby, G. H., Hunter, D. A., & Christian, C. A. 1984, *ApJS*, 56, 257
- Jester, S., Schneider, D. P., Richards, G. T., et al. 2005, *AJ*, 130, 873
- Jones, J. E., Alloin, D. M., & Jones, B. J. T. 1984, *ApJ*, 283, 457
- Johnston, H. M., Wu, K., Fender, R., & Cullen, J. G. 2001, *MNRAS*, 328, 1193
- Jonker, P. G., Nelemans, G., Bassa, C. G., *MNRAS*, 374, 999
- Jonker, P. G., Bassa, C. G., Nelemans, G., et al. 2011, *ApJS*, 194, 18
- Jonker, P. G., Miller-Jones, J. C. A., Homan, J., et al. 2012, *MNRAS*, 423, 3308
- Kafka, S., Honeycutt, R. K., Howell, S. B., & Harrison, T. E. 2005, *AJ*, 130, 2852
- Kirkpatrick, J. D., Henry, T. J., & McCarthy, D. W., Jr. 1991, *ApJS*, 77, 417
- Kirkpatrick, J. D., Kelly, D. M., Rieke, G. H., et al. 1993, *ApJ*, 402, 643
- Knigge, C. 2006, *MNRAS*, 373, 484
- Kolb, U., Davies, M. B., King, A., & Ritter, H. 2000, *MNRAS*, 317, 438
- Le Fèvre, O., Saisse, M., Mancini, D., et al. 2003, *Proc. SPIE*, 4841, 1670
- Lindström, C., Griffin, J., Kiss, L. L., et al. 2005, *MNRAS*, 363, 882
- Maccarone, T. J., Bandyopadhyay, R., Kennea, J., et al. 2012a, *The Astronomer's Telegram*, 4109, 1
- Maccarone, T. J., Torres, M. A. P., Britt, C. T., et al. 2012b, *MNRAS*, 426, 3057
- Marsh, T. R., Robinson, E. L., & Wood, J. H. 1994, *MNRAS*, 266, 137
- Mignani, R., Caraveo, P. A., & Bignami, G. F. 1997, *A&A*, 323, 797
- Mohanty, S., & Basri, G. 2003, *ApJ*, 583, 451
- Munari, U., & Tomasella, L. 1999, *A&AS*, 137, 521
- Munari, U. 2000, *Molecules in Space and in the Laboratory*, 179
- Naylor, T., Allan, A., & Long, K. S. 2005, *MNRAS*, 361, 1091
- Nelemans, G., Jonker, P. G., Marsh, T. R., & van der Klis, M. 2004, *MNRAS*, 348, L7
- Nelemans, G., Jonker, P. G., & Steeghs, D. 2006, *MNRAS*, 370, 255
- Orosz, J. A., & Bailyn, C. D. 1997, *ApJ*, 477, 876
- Orosz, J. A., Jain, R. K., Bailyn, C. D., McClintock, J. E., & Remillard, R. A. 1998, *ApJ*, 499, 375
- Osterbrock, D. E., Fulbright, J. P., Martel, A. R., et al. 1996, *PASP*, 108, 277
- Osterbrock, D. E., Fulbright, J. P., & Bida, T. A. 1997, *PASP*, 109, 614
- Özel, F., Psaltis, D., Narayan, R., & McClintock, J. E. 2010, *ApJ*, 725, 1918
- Ramsay, G., & Wheatley, P. J. 1998, *MNRAS*, 301, 95
- Ratti, E. M., Steeghs, D. T. H., Jonker, P. G., et al. 2012, *MNRAS*, 420, 75
- Ratti, E. M., van Grunsven, T. F. J., Jonker, P. G., et al. 2013a, *MNRAS*, 428, 3543
- Ratti, E. M., van Grunsven, T. F. J., Torres, M. A. P., et al. 2013b, *arXiv:1301.4896*
- Reipurth, B., Pedrosa, A., & Lago, M. T. V. T. 1996, *A&AS*, 120, 229
- Reis, R. C., Wheatley, P. J., Gänsicke, B. T., & Osborne, J. P. 2013, *MNRAS*, 430, 1994
- Rodríguez-Gil, P., Schmidtobreick, L., Gaumlinckic, B. T. 2007a, *MNRAS*, 374, 1359
- Rodríguez-Gil, P., Gänsicke, B. T., Hagen, H.-J., et al. 2007, *MNRAS*, 377, 1747
- Rodríguez-Gil, P., Schmidtobreick, L., Long, K. S., et al. 2012a, *MNRAS*, 422, 2332
- Rodríguez-Gil, P., Schmidtobreick, L., Long, K. S., et al. 2012b, *Memorie della Societa Astronomica Italian*, 83, 602
- Roeser, S., Demleitner, M., & Schilbach, E. 2010, *AJ*, 139, 2440
- Rojas, A. F., Greiss, S., Masetti, N., Steeghs, D., & Minniti, D. 2012, *The Astronomer's Telegram*, 4006, 1
- Sakano, M., Koyama, K., Murakami, H., Maeda, Y., & Yamauchi, S. 2002, *ApJS*, 138, 19
- Shahbaz, T., van der Hooft, F., Casares, J., Charles, P. A., & van Paradijs, J. 1999, *MNRAS*, 306, 89
- Shears, J., Boyd, D., & Poyner, G. 2006, *Journal of the British Astronomical Asso*
- Schoembs, R., & Hartmann, K. 1983, *A&A*, 128, 37
- Shaw, R. A. (ed.) 2009, *NOAO Data Handbook (Version 1.1; Tucson; National Optical Astronomical Observatory)*
- Skidmore, W., Mason, E., Howell, S. B., et al. 2000, *MNRAS*, 318, 429
- Telleschi, A., Güdel, M., Briggs, K. R., Audard, M., & Palla, F. 2007, *A&A*, 468, 425
- Thomas, H.-C., Beuermann, K., Reinsch, K., Schwöpe, A. D., & Burwitz, V. 2012, *A&A*, 546, A104
- Torres, M. A. P., Casares, J., Martínez-Pais, I. G., & Charles, P. A. 2002, *MNRAS*, 334, 233
- Torres, M. A. P., Garcia, M. R., Steeghs, D., & McClintock, J. E. 2005, *ApJ*, 632, 514
- Udalski, A., Kowalczyk, K., Soszyński, I., et al. 2012, *AcA*, 62, 133
- van Paradijs, J., Augusteijn, T., & Stehle, R. 1996, *A&A*, 312, 93
- van Spaandonk, L., Steeghs, D., Marsh, T. R., & Torres, M. A. P. 2010, *MNRAS*, 401, 1857
- Walter, F. M., & Basri, G. S. 1982, *ApJ*, 260, 735
- Wang, Z., Archibald, A. M., Thorstensen, J. R., et al. 2009, *ApJ*, 703, 2017
- Werner, K., Nagel, T., Rauch, T., Hammer, N. J., & Dreizler, S. 2006, *A&A*, 450, 725
- Williams, K. A., Howell, S. B., Liebert, J., et al. 2013, *AJ*, 145, 129
- Zhou, X. 1991, *A&A*, 248, 367

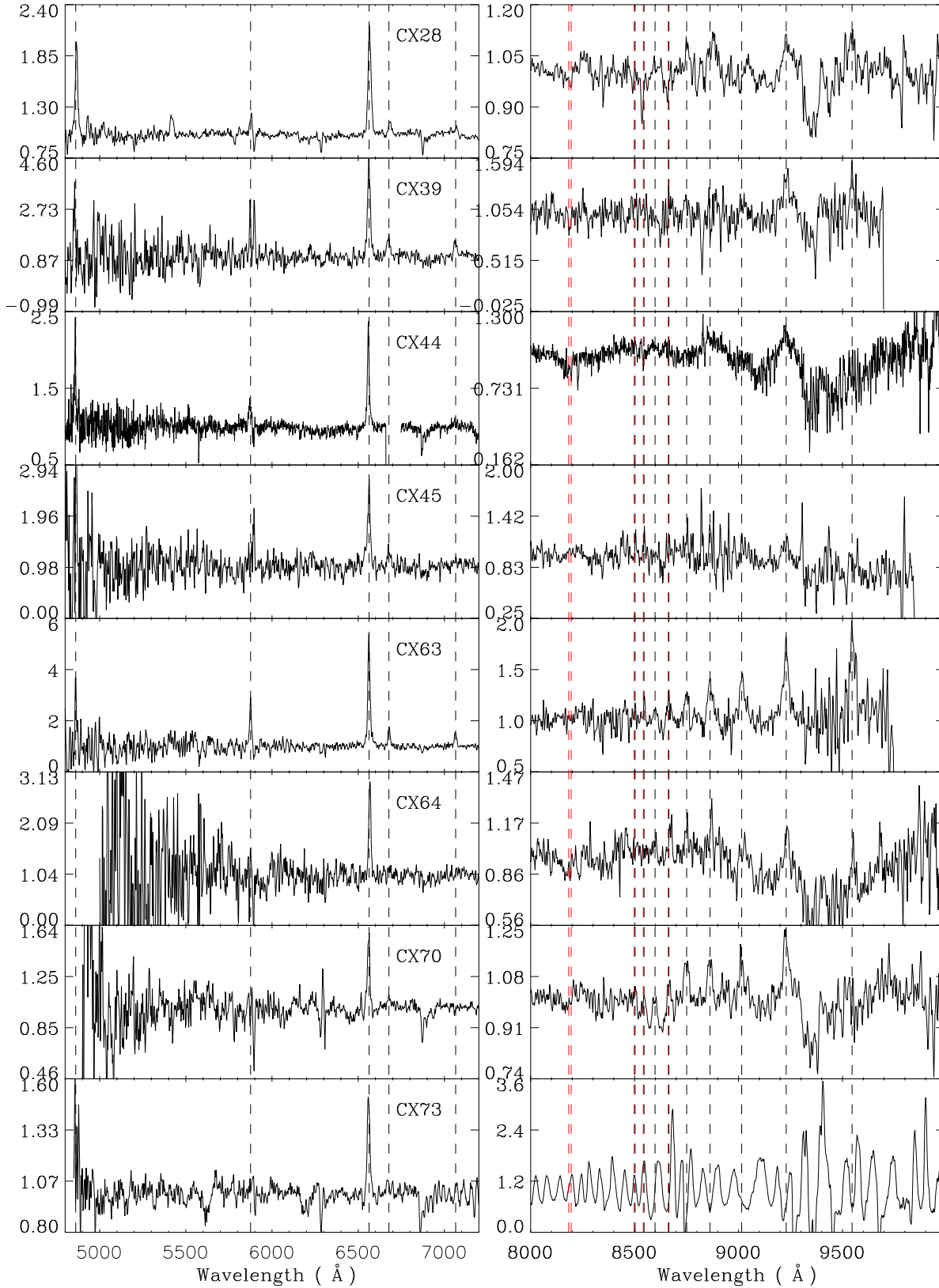


Figure 1. Continuum-normalized spectra of GBS sources in two wavelength ranges. The rest wavelnths for the lines given in Sec 3.1 are marked with black dashed lines except the Ca II IR triplet (red dashed lines). Note that the P13, 15 and 16 Paschen lines are blended with the Ca triplet.

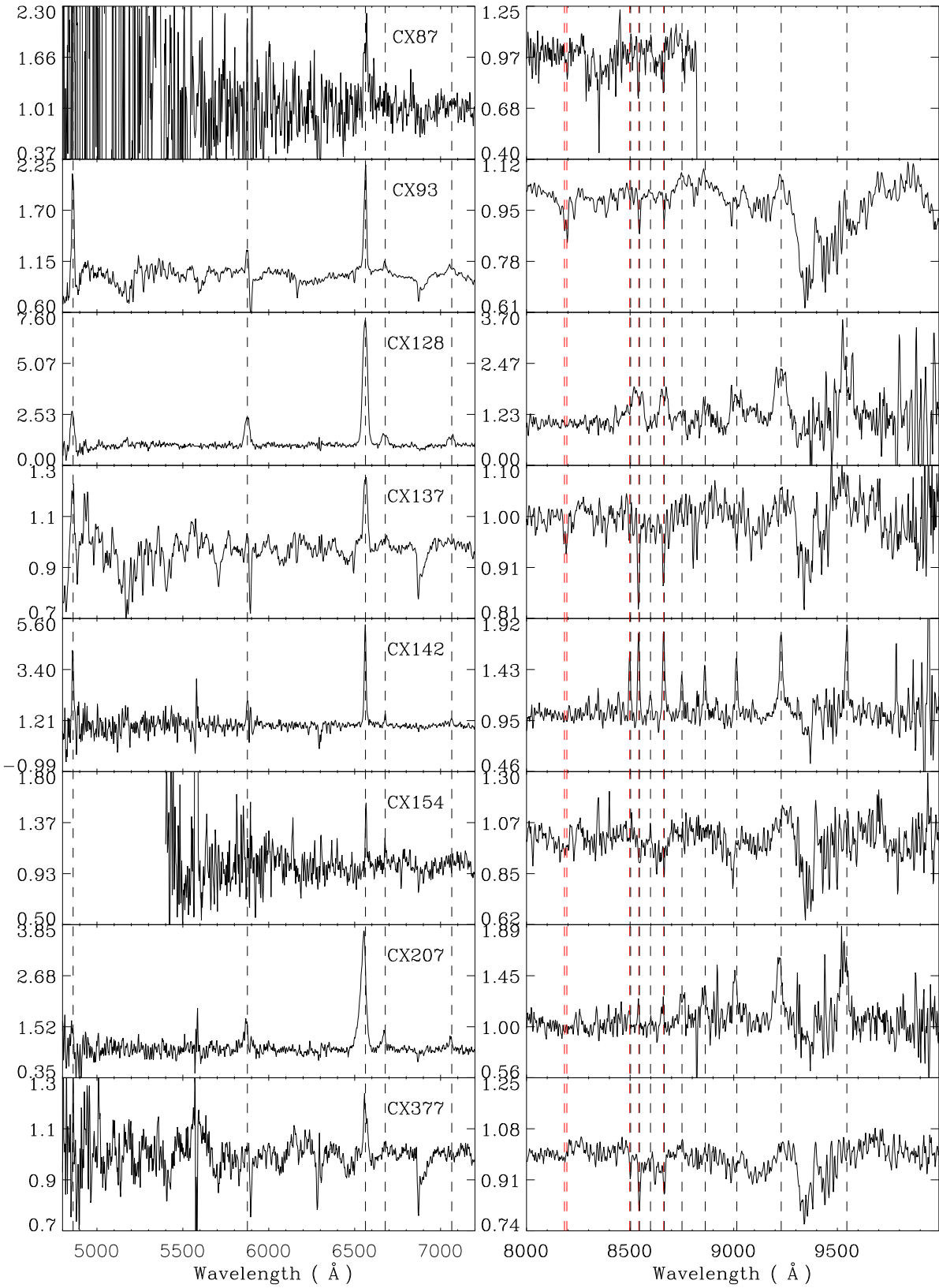


Figure 2. Normalized spectra of GBS sources (continued).

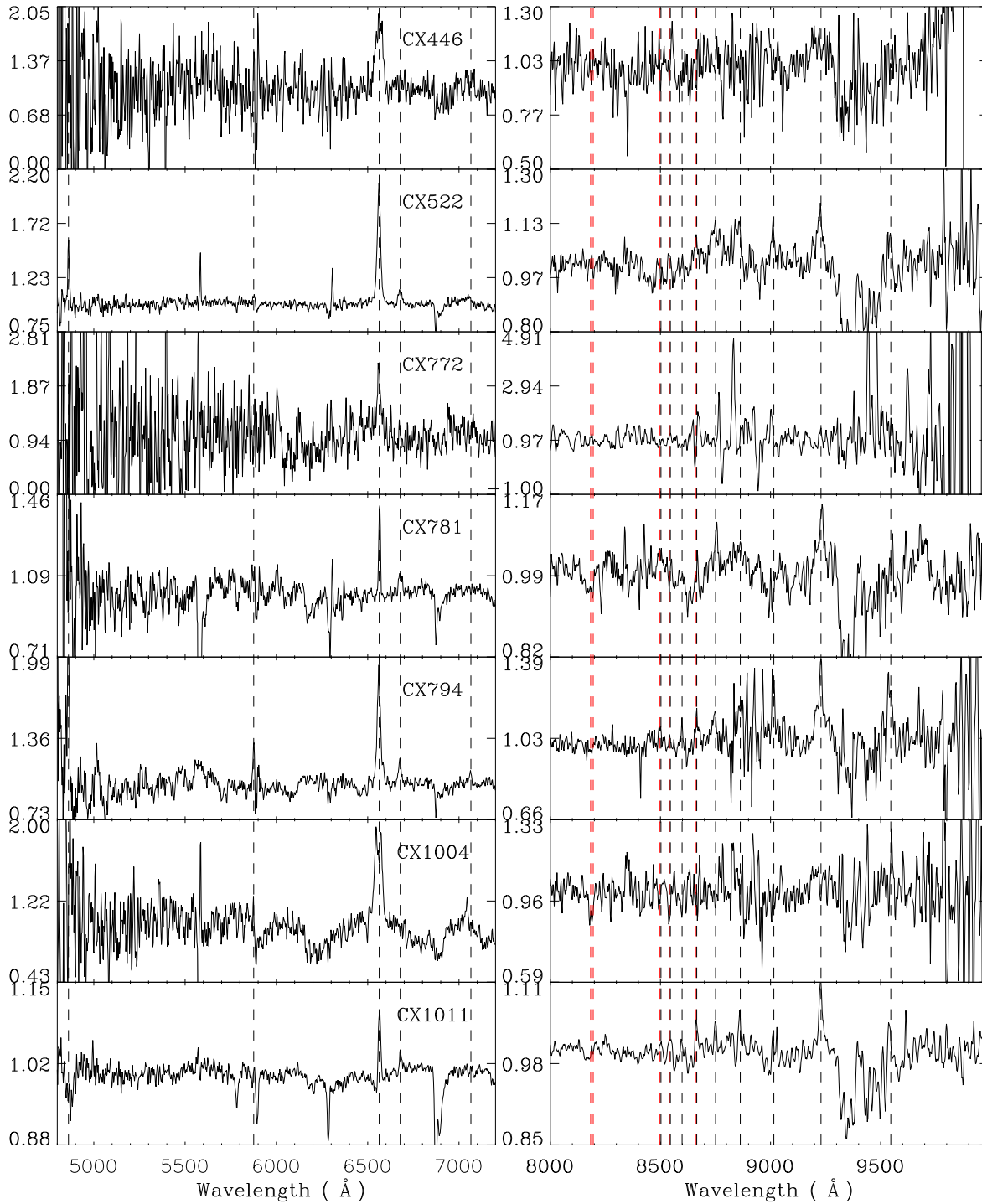


Figure 3. Normalized spectra of GBS sources (continued).

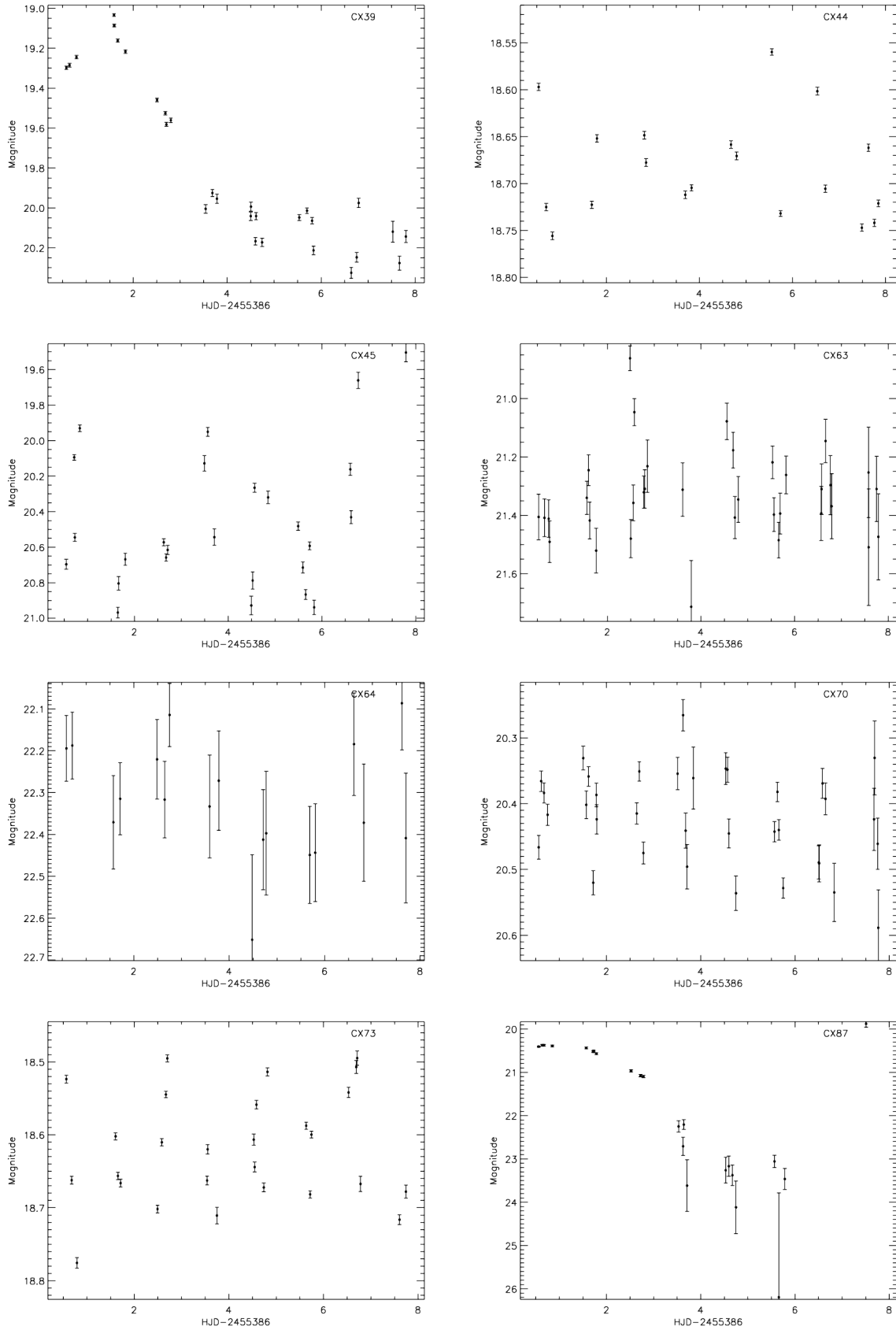


Figure 4. Optical light curves for 20 of the 23 accreting binaries reported in this paper. The light curves for CX28 and CX93 can be found in Britt et al. (2013) and Ratti et al. (2012a). No suitable data was available to obtain a light curve for CX522.

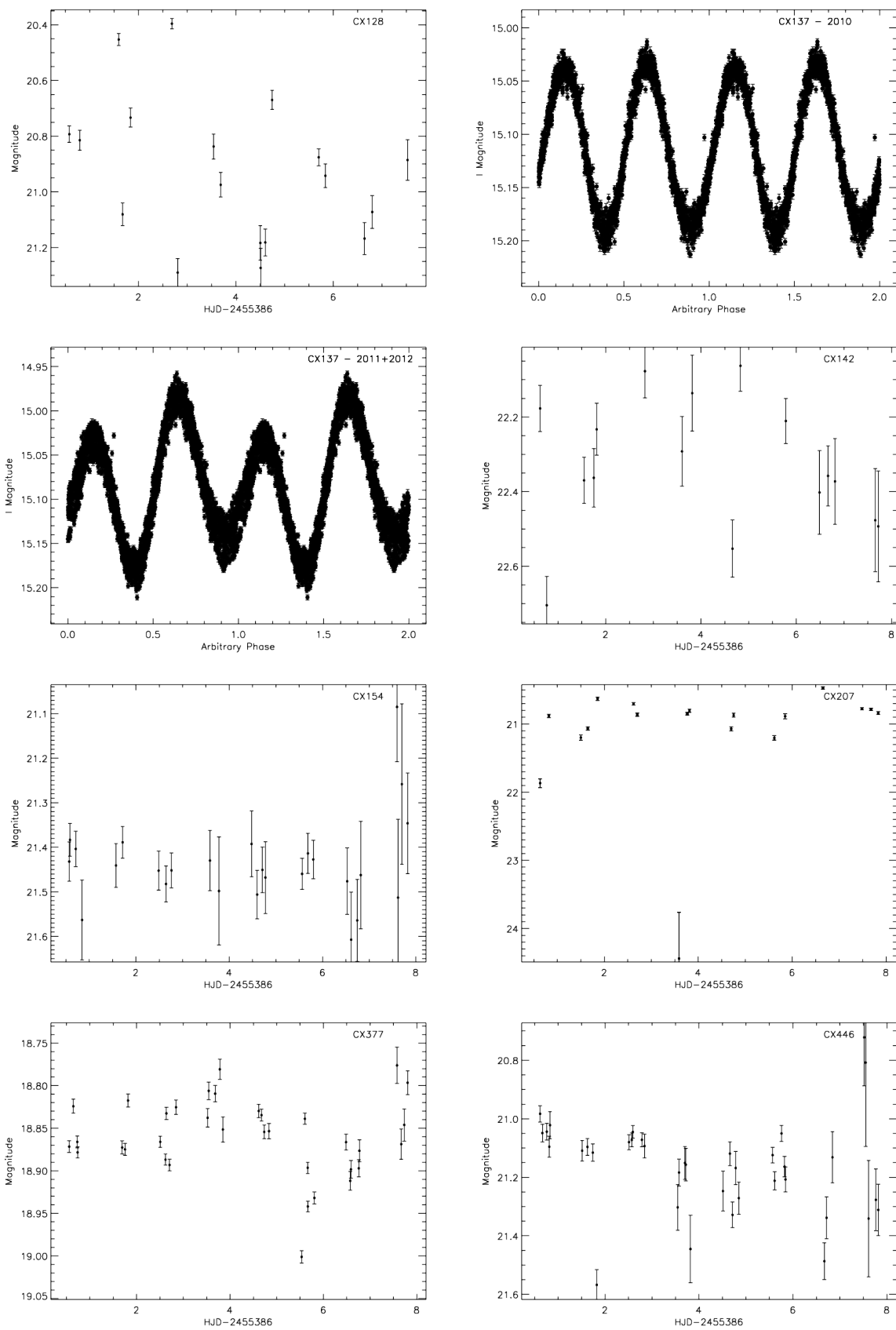


Figure 5. Optical light curves (continued). The CX137 light curves are based on OGLE-IV data.

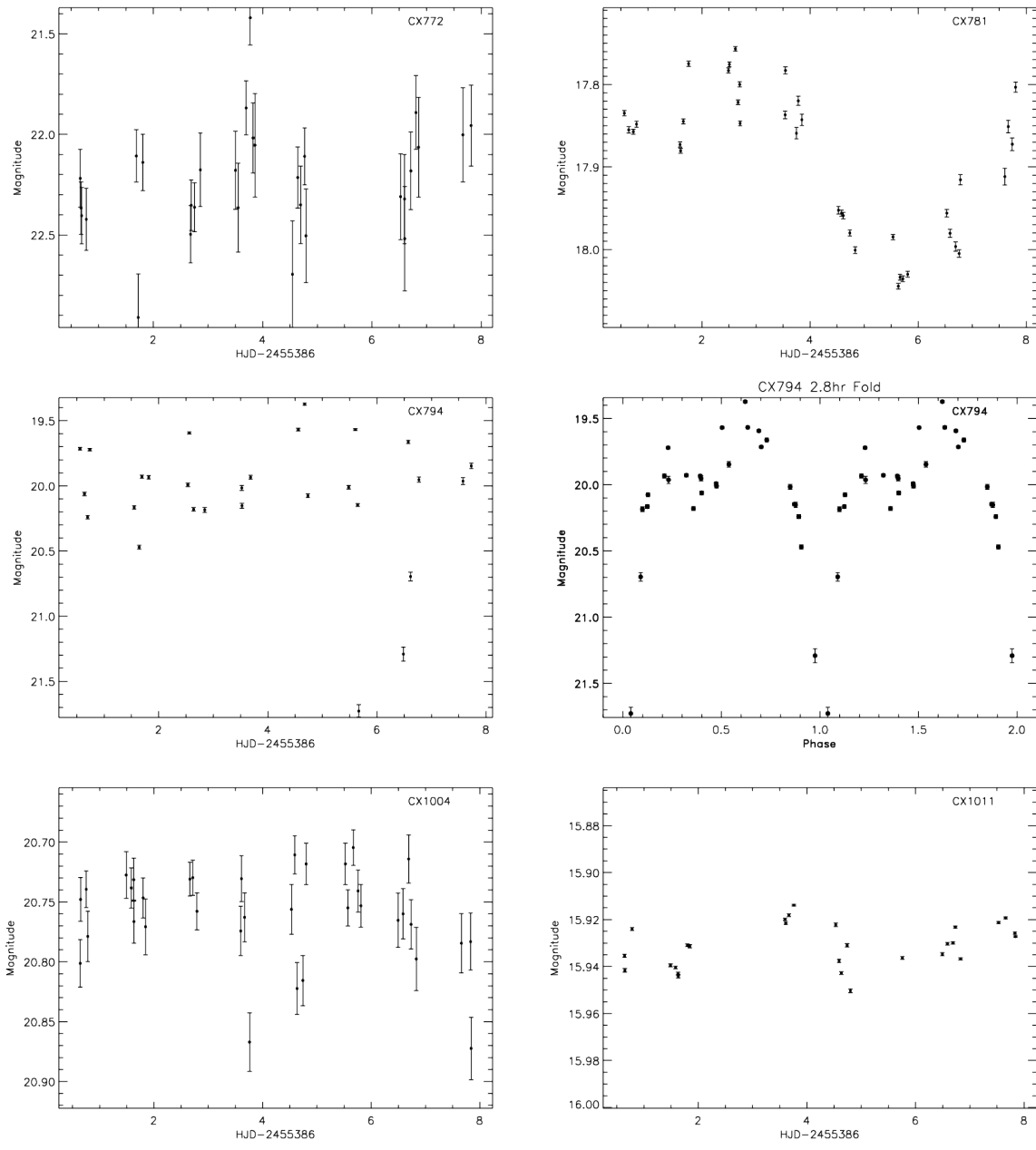


Figure 6. Optical light curves (continued). The Mosaic-II light curve of CX794 is also shown folded on the ephemeris of Section N.

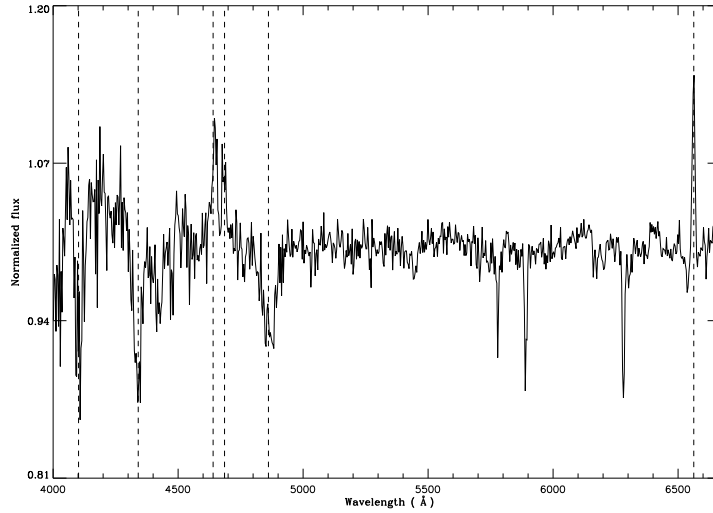


Figure 7. Normalized IMACS spectrum of CX1011. Markers are for $H\delta$, $H\gamma$, the Bowen blend, $\text{HeII } \lambda 4686$, $H\beta$ and $H\alpha$. The three prominent absorption features in the region $\lambda\lambda 5800 - 6300$ are interstellar in origin.

Table 1. A log of the VIMOS and Mosaic-II observations.

| GBS No | VIMOS OB ID (spectroscopy) | VIMOS OB ID (pre-imaging) | VIMOS Quadrant | Date UT (spectroscopy) | Mosaic-II N frames |
|--------|----------------------------|---------------------------|----------------|------------------------|--------------------|
| CX28 | 453466 | 509361 | 4 | 2011-04-02 | 28 |
| CX39 | 508808 | 453460 | 1 | 30-03-2011 | 29 |
| CX45 | 575808 | 453494 | 1 | 04-07-2011 | 26 |
| CX63 | 575585 | 453506 | 2 | 30-06-2011 | 35 |
| CX64 | 575148 | 453474 | 3 | 09-06-2011 | 18 |
| CX70 | 577698 | 453498 | 1 | 01-07-2011 | 35 |
| CX73 | 484756 | 453436 | 2 | 09-05-2010 | 27 |
| CX87 | 575612 | 453490 | 2 | 03-07-2011 | 21 |
| CX93 | 509202 | 453434 | 2 | 29-04-2011 | 35 |
| CX128 | 509361 | 453466 | 2 | 02-04-2011 | 18 |
| CX137 | 577805 | 544378 | 1 | 22-07-2011 | 4 |
| CX142 | 577743 | 544353 | 4 | 26-06-2011 | 16 |
| CX154 | 575008 | 453472 | 3 | 26-05-2011 | 26 |
| | 575148 | 453474 | 2 | 09-06-2011 | |
| CX207 | 508997 | 453430 | 2 | 02-05-2011 | 35 |
| | 575272 | 453430 | 2 | 06-06-2011 | |
| CX377 | 575026 | 453452 | 1 | 28-05-2011 | 35 |
| | 575799 | 453452 | 1 | 23-07-2011 | |
| CX446 | 508787 | 453428 | 1 | 02-05-2011 | 37 |
| CX522 | 575918 | 544379 | 4 | 04-08-2011 | — |
| CX772 | 484978 | 453440 | 2 | 11-05-2010 | 30 |
| CX781 | 575403 | 453446 | 2 | 27-07-2011 | 38 |
| CX794 | 509817 | 453456 | 1 | 03-04-2011 | 28 |
| | 575275 | 453456 | 1 | 26-05-2011 | |
| CX1004 | 577836 | 544354 | 2 | 28-06-2011 | 35 |
| CX1011 | 577836 | 544354 | 4 | 28-06-2011 | 28 |

Table 2. Spectroscopic measurements. An * indicates that the measured EW is most likely a lower limit due to contamination of unresolved star/s during the extraction of the spectra.

| GBS No | α (deg) | δ (deg) | r' | Remarks |
|--------------------|----------------|---------------------|-----------------------|--|
| Specie λ_0 | RV (km/s) | EW (\AA) | FWHM (\AA) | |
| CX28* | 264.94581 | -27.302481 | 16.89 ± 0.20 | |
| HeII 4686.75 | 420 ± 30 | 23 ± 3 | 19.2 ± 0.7 | High accretion rate CV |
| H I 4861.327 | 320 ± 20 | 13.4 ± 0.5 | 14.3 ± 0.5 | |
| HeII 5411.551 | 330 ± 20 | 5.1 ± 0.3 | 22.3 ± 0.7 | |
| HeI 5875.618 | 150 ± 20 | 3.9 ± 0.1 | 16.1 ± 0.3 | |
| H I 6562.76 | 150 ± 10 | 22.5 ± 0.9 | 19.8 ± 0.2 | |
| HeI 6678.149 | 300 ± 20 | 3.4 ± 0.5 | 21.4 ± 0.2 | |
| CX39* | 265.4167 | -27.293809 | 19.8 ± 0.4 | |
| H I 6562.76 | -5 ± 4 | 86 ± 4 | 20 ± 1 | Outbursting CV |
| HeI 6678.149 | 151 ± 9 | 15 ± 1 | 21.2 ± 0.8 | |
| HeI 7065.188 | -50 ± 20 | 11.4 ± 0.5 | 19.4 ± 0.7 | |
| CX44 | 268.92844 | -28.302561 | 18.68 ± 0.05 | |
| H I 4861.327 | -190 ± 20 | 11 ± 1 | 9 ± 2 | Quiescent neutron star LMXB or low accretion rate CV |
| HeI 5875.618 | -170 ± 40 | 5.8 ± 0.5 | 21.0 ± 0.7 | |
| H I 6562.76 | -240 ± 9 | 20 ± 1 | 13.4 ± 0.1 | |
| CX45 | 263.9106 | -28.881169 | 20.4 ± 0.3 | |
| H I 6562.76 | -48 ± 4 | 40 ± 3 | 21.6 ± 0.3 | CV with accretion-dominated optical spectrum |
| HeI 6678.149 | -2 ± 16 | 8.5 ± 0.2 | 20.9 ± 0.9 | |
| CX63* | 263.54742 | -29.521676 | 21.3 ± 0.2 | |
| H I 4861.327 | -63 ± 4 | $\gtrsim 35 \pm 2$ | $\gtrsim 9 \pm 1$ | CV with accretion-dominated optical spectrum |
| HeI 5875.618 | -13 ± 5 | 31 ± 8 | 12.1 ± 0.9 | |
| H I 6562.76 | -45 ± 2 | 65 ± 2 | 14.8 ± 0.1 | |
| HeI 6678.149 | 13 ± 4 | 9.8 ± 0.1 | 13.4 ± 0.5 | |
| HeI 7065.188 | -60 ± 10 | 9.0 ± 0.3 | 14.6 ± 0.5 | |
| H I 8665.019 (P13) | -30 ± 10 | 4.7 ± 0.9 | 20.8 ± 0.9 | |
| H I 8750.473 (P12) | -2 ± 7 | 8.8 ± 0.4 | 23.5 ± 0.9 | |
| H I 8862.784 (P11) | 50 ± 30 | 14.6 ± 2.4 | 32 ± 4 | |
| H I 9014.911 (P10) | 50 ± 20 | 9.6 ± 1.7 | 22.0 ± 0.9 | |
| H I 9229.015 (P9) | -30 ± 6 | 18.1 ± 0.7 | 28.1 ± 0.5 | |
| CX64 | 264.51153 | -28.523984 | 22.3 ± 0.1 | |
| H I 6562.76 | 212 ± 2 | 33 ± 1 | 14.8 ± 0.1 | CV in a low state of accretion or CV in the Bulge region |
| CX70 | 263.89611 | -29.994897 | 20.42 ± 0.07 | |
| H I 6562.76 | -133 ± 2 | 15 ± 1 | 20.3 ± 0.2 | CV with accretion-dominated optical spectrum |
| H I 8598.392 (P14) | -70 ± 20 | 2.9 ± 0.1 | 25.0 ± 0.2 | |
| H I 8665.019 (P13) | 61 ± 7 | 3.6 ± 0.3 | 23 ± 2 | |
| H I 8750.473 (P12) | -90 ± 10 | 4.0 ± 0.2 | 27.6 ± 0.8 | |
| H I 8862.784 (P11) | 30 ± 40 | 3.6 ± 0.4 | 25 ± 1 | |
| CX73 | 266.19797 | -27.017144 | 18.62 ± 0.08 | |
| H I 6562.76 | -116 ± 4 | 11.4 ± 0.2 | 18.8 ± 0.4 | Unknown nature |

Table 3. Spectroscopic measurements (continued).

| GBS No | α (deg) | δ (deg) | r' | Remarks |
|---------------------------|------------------|-----------------------|------------------------|--|
| Specie λ_0 | RV (km/s) | EW (\AA) | FWHM (\AA) | |
| CX87 | 264.20005 | -29.611037 | ~ 23.3 | |
| H α 6562.76 | 50 ± 50 | 24 ± 5 | 27 ± 3 | Outbursting CV |
| CX93 | 266.18661 | -26.058373 | 17.07 ± 0.03 | |
| H α 4861.327 | -70 ± 20 | 27 ± 2 | 16.7 ± 0.2 | Low accretion rate CV |
| He α 5875.618 | -60 ± 10 | 5.0 ± 0.5 | 15.5 ± 0.4 | |
| H α 6562.76 | -17 ± 4 | 18.4 ± 0.3 | 16.7 ± 0.3 | |
| He α 6678.149 | -64 ± 2 | 1.6 ± 0.2 | 18.2 ± 0.4 | |
| CX128* | 265.11822 | -27.193451 | 20.9 ± 0.3 | |
| H α 4861.327 | -180 ± 60 | 91 ± 5 | 26.2 ± 0.8 | CV with disc-dominated optical spectrum, likely short orbital period dwarf nova |
| He α 5875.618 | -30 ± 20 | 56 ± 5 | 33 ± 1 | |
| H α 6562.760 | -70 ± 4 | 197 ± 7 | 31.0 ± 0.2 | |
| He α 6678.149 | -180 ± 10 | 20 ± 1 | 35.5 ± 0.4 | |
| He α 7065.188 | -110 ± 40 | 20 ± 1 | 44 ± 4 | |
| H α 8545.383 (P15) | -180 ± 10 | 69 ± 7 | 61 ± 4 | |
| H α 8665.019 (P13) | -20 ± 10 | 48 ± 4 | 46.6 ± 0.7 | |
| H α 9014.911 (P10) | -130 ± 30 | 45 ± 2 | 58 ± 3 | |
| H α 9229.015 (P9) | -40 ± 20 | 100 ± 30 | 65 ± 3 | |
| CX137* | 268.97196 | -28.276046 | 16.14 ± 0.01 | |
| H α 6562.76 | -9 ± 9 | $\gtrsim 6.5 \pm 0.2$ | $\gtrsim 23.4 \pm 0.4$ | Low accretion rate CV or qLMXB?, $P_{orb} = 0.431$ d |
| CX142 | 266.01566 | -31.384838 | 22.3 ± 0.2 | |
| H α 4861.327 | -90 ± 10 | 120 ± 80 | 14 ± 2 | CV with accretion-dominated optical spectrum |
| He α 5875.618 | — | — | — | |
| H α 6562.76 | -69 ± 1 | 59 ± 4 | 12.4 ± 0.2 | |
| He α 6678.149 | -28 ± 9 | 4.9 ± 0.3 | 9 ± 1 | |
| He α 7065.188 | -42 ± 8 | 6.2 ± 0.4 | 16.0 ± 0.9 | |
| Ca α 8498.02 + P16 | 0 ± 10 | 8.0 ± 0.4 | 10.4 ± 0.3 | |
| Ca α 8542.09 + P15 | -39 ± 2 | 10.8 ± 0.3 | 1.1 ± 0.3 | |
| H α 8598.392 (P14) | -10 ± 20 | 4.2 ± 0.6 | 13.3 ± 0.5 | |
| Ca α 8662.14 + P13 | -7 ± 2 | 9.2 ± 0.3 | 11.1 ± 0.4 | |
| H α 8750.473 (P12) | -37 ± 7 | 4.8 ± 0.2 | 11.0 ± 0.3 | |
| H α 8862.784 (P11) | -68 ± 7 | 7 ± 1 | 14 ± 2 | |
| H α 9014.911 (P10) | -54 ± 7 | 8.0 ± 0.4 | 12.8 ± 0.7 | |
| H α 9229.015 (P9) | -31 ± 7 | 11 ± 1 | 17 ± 1 | |
| H α 9545.972 (P8) | -44 ± 7 | 10.2 ± 0.6 | 13.6 ± 0.2 | |
| CX154* | 264.66119 | -28.594338 | 21.4 ± 0.1 | |
| H α 6562.76 | 1 95 ± 9 | 8 ± 2 | 11.3 ± 0.8 | Low accretion rate CV or qLMXB |
| | 2 142 ± 4 | 7.6 ± 0.4 | 8.5 ± 0.5 | |
| He α 6678.149 | 2 10 ± 9 | 2.8 ± 0.4 | 12.7 ± 0.4 | (1,2: 2011 May 26, Jun 9) |
| CX207* | 266.60619 | -26.526381 | 21.1 ± 0.9 | |
| He α 5875.618 | 1 -370 ± 20 | 14 ± 2 | 22 ± 1 | Eclipsing high accretion rate CV, most likely a magnetic (Polar) CV (1,2: 2011 May 2, Jun 6) |
| | 2 -210 ± 50 | 21 ± 2 | 41 ± 4 | |
| H α 6562.76 | 1 -558 ± 4 | 107 ± 8 | 37.7 ± 0.7 | |
| | 2 -358 ± 4 | 83 ± 9 | 35.1 ± 0.6 | |
| He α 6678.149 | 1 -330 ± 10 | 10 ± 1 | 22.0 ± 0.8 | |
| | 2 -200 ± 100 | 7 ± 1 | 32 ± 5 | |
| He α 7065.188 | 1 -250 ± 10 | 6.8 ± 0.6 | 22 ± 2 | |
| | 2 -190 ± 30 | 6.5 ± 0.3 | 38 ± 2 | |

Table 4. Spectroscopic measurements (continued).

| GBS No | | α (deg) | δ (deg) | r' | Remarks |
|-----------------------------|---|----------------|---------------------|-----------------------|--|
| Specie λ_0 | | RV (km/s) | EW (\AA) | FWHM (\AA) | |
| CX207* | | (continued) | | | |
| H I 8665.019 (P13) | 1 | -280 ± 10 | 3.2 ± 0.4 | 16 ± 1 | |
| H I 8862.784 (P11) | 1 | -200 ± 30 | 8 ± 3 | 29 ± 3 | |
| H I 9014.911 (P10) | 1 | -280 ± 20 | 7.7 ± 0.9 | 19.5 ± 0.8 | |
| H I 9229.015 (P9) | 1 | -330 ± 30 | 23 ± 6 | 39 ± 8 | |
| | 2 | -180 ± 30 | 33 ± 3 | 55 ± 3 | |
| H I 9545.972 (P8) | 1 | -460 ± 30 | 37 ± 9 | 46 ± 2 | |
| CX377* | | 265.8189 | -27.760333 | 18.86 ± 0.05 | |
| H I 6562.76 | 1 | 30 ± 30 | 6.6 ± 0.3 | 29 ± 2 | Low accretion rate CV or qLMXB, (1,2: 2011 Jul 23, Aug 28) |
| | 2 | -39 ± 4 | 6.4 ± 0.2 | 27.3 ± 0.6 | |
| CX446 | | 266.61317 | -25.83124 | 21.2 ± 0.2 | |
| H I 6562.76 | | -10 ± 20 | 50 ± 4 | 49 ± 1 | High inclination CV or qLMXB |
| CX522 | | 268.63525 | -28.488483 | — | |
| H I 4861.327 | | 42.0 ± 0.1 | 6 ± 1 | 10 ± 1 | CV of unknown type |
| He I 5875.618 | | 30 ± 70 | 1.2 ± 0.2 | 16 ± 3 | |
| H I 6562.76 | | -84 ± 1 | 23.3 ± 0.9 | 21.1 ± 0.2 | |
| He I 6678.149 | | -80 ± 40 | 3.2 ± 0.3 | 25 ± 2 | |
| CX772 | | 266.02105 | -26.533196 | 22.2 ± 0.3 | |
| H I 6562.76 | | -40 ± 20 | 24 ± 4 | 22 ± 4 | Unknown nature |
| CX781 | | 265.79638 | -27.272705 | 17.89 ± 0.09 | |
| H I 6562.76 | | 102 ± 1 | 5.0 ± 0.2 | 10.1 ± 0.2 | CV with accretion-dominated optical spectrum |
| He I 6678.149 | | 10 ± 30 | 2.3 ± 0.2 | 24 ± 2 | |
| CX794 | | 265.42652 | -27.975019 | 20.1 ± 0.5 | |
| H I 4861.327 | | -10 ± 10 | 13 ± 1 | 9.8 ± 0.7 | High accretion rate CV eclipsing, $P_{orb} = 0.11786$ d |
| H I 6562.76 | | -69 ± 4 | 23 ± 1 | 23.0 ± 0.4 | |
| He I 6678.149 | | -80 ± 20 | 5 ± 2 | 19 ± 2 | |
| CX1004 | | 266.59799 | -31.09717 | 20.75 ± 0.04 | |
| H I 6562.76 | | -210 ± 20 | 32.9 ± 0.4 | 46.4 ± 0.4 | Low accretion rate eclipsing CV or qLMXB |
| CX1011 | | 266.51968 | -31.289612 | 15.93 ± 0.01 | |
| H I 6562.76 | 1 | 18 ± 6 | 2.36 ± 0.04 | 13.59 ± 0.04 | High accretion rate CV, nova-like (1,2: 2011 May 13, Jun 28) |
| | 2 | 93 ± 5 | 2.14 ± 0.07 | 15.1 ± 0.2 | |
| He I 6678.149 | 2 | 40.2 ± 10 | 0.46 ± 0.04 | 13.3 ± 0.5 | |
| H I 9229.015 (P9) | 2 | 50 ± 10 | 1.5 ± 0.1 | 16.7 ± 0.5 | |

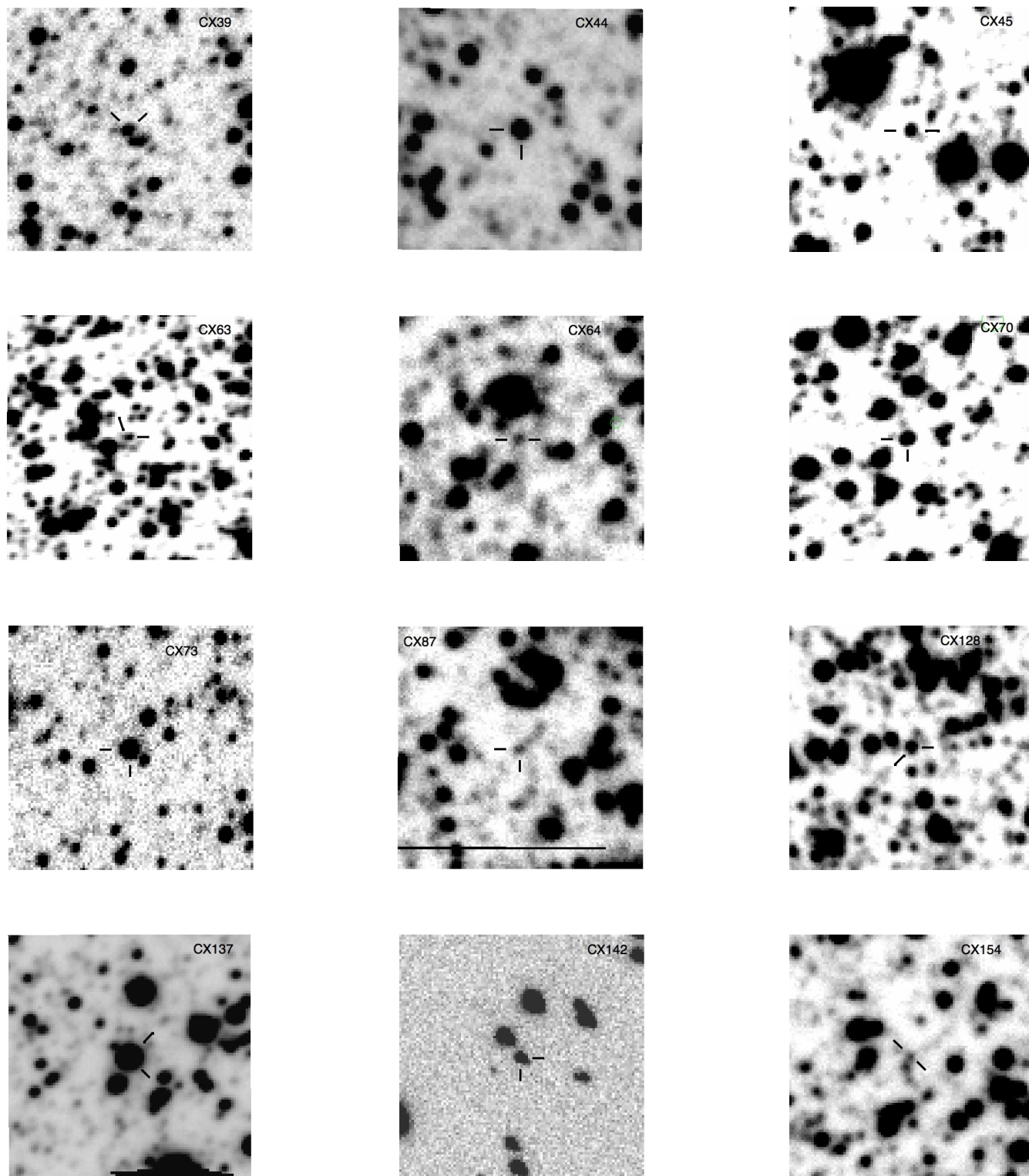


Figure 8. Finding charts.

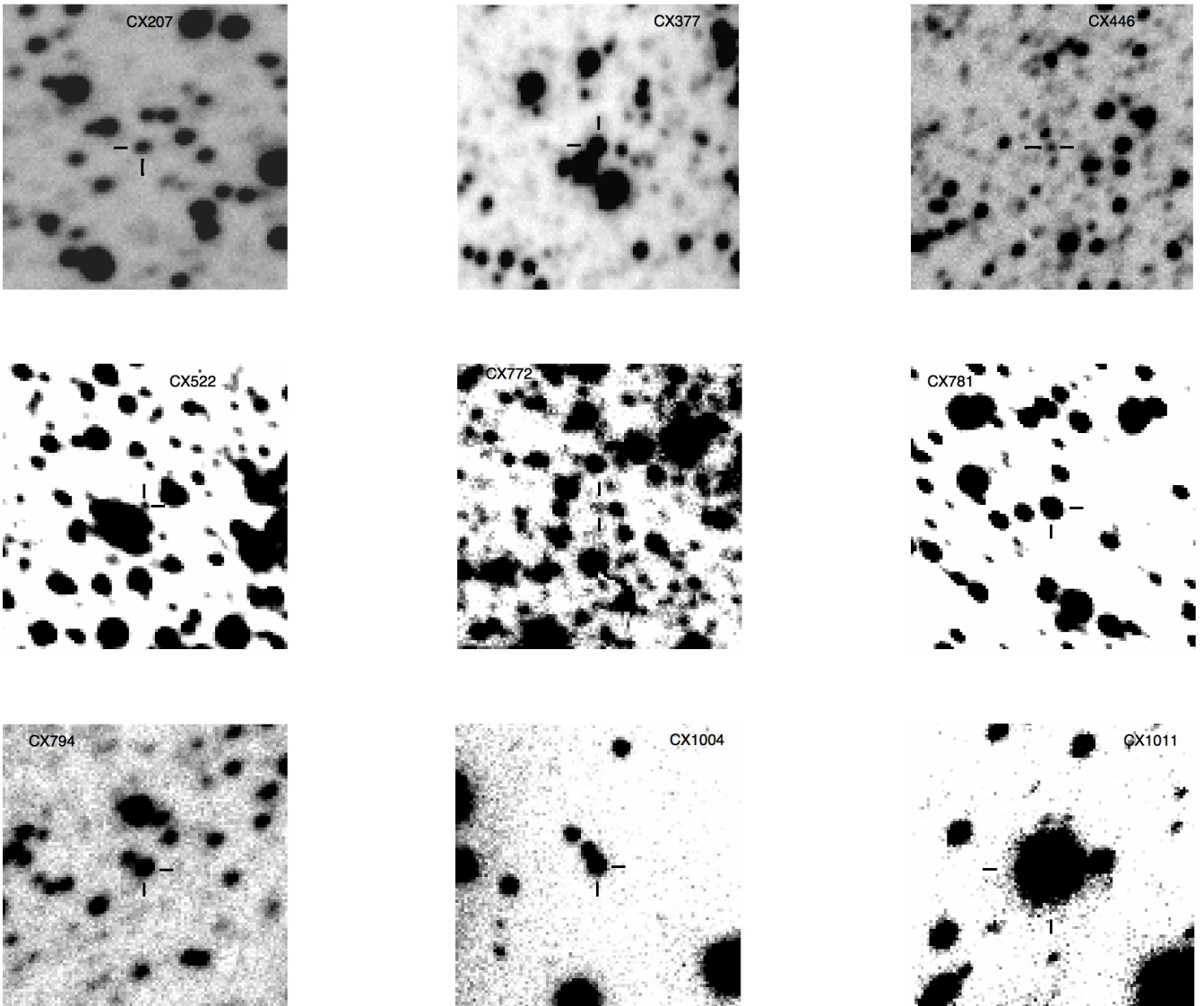


Figure 9. Finding charts (continued).